Learning Therapist's Intervention from Demonstration: Application for Robotic Assistance to Children with Cerebral Palsy

by

Mohammad Najafi

A thesis submitted in partial fulfillment of the requirements for the degree of

Master of Science

in

Control Systems

Department of Electrical and Computer Engineering

University of Alberta

Abstract

Physical interaction with the environment and object manipulation play an important role in the development of children's cognitive and perceptual skills. For children who have severe physical impairments, one of the biggest concerns is the loss of opportunities for play. Robots can be used to build function so children can independently engage in activities (e.g., rehabilitation robots), or to compensate for function (e.g., assistive robots). The main focus of this thesis is development, analysis and implementation of user-friendly *Learning from Demonstration* frameworks that teach the robots the required task-specific assistance by a few demonstrations from an expert helper (in rehabilitation scenarios it could be a therapist helping a patient, at home it could be a parent or sibling helping a child), and eliminate the requirement for manual robot programming. The terms therapist and patient will be used throughout this thesis but the robotic assistance can apply to both rehabilitation and compensation robots.

The proposed learning from demonstration frameworks in this paper consists of three phases: 1) *Demonstration phase*: The therapist interacts with the patient and provides the required assistance to the robot to perform and complete the task successfully for one or more trials; 2) *Learning phase*: Machine

learning algorithms model the assistance provided by the therapist and program the robot controllers accordingly to provide the same encoded assistance to the patient in the therapist's absence; and 3) *Robotic assistance phase*: The robotic system independently provides the learned assistance to the patient, with an interactive mechanism to regulate human-robot cooperation.

In this thesis, the *task* is considered as point-to-point motion (also called reaching motion) primitives which are the building blocks for most of our daily activities. Two class of learning from demonstration frameworks have been proposed in this thesis that uses either *time-indexed* or *position-indexed* approaches to learn and reproduce the assistance in a point-to-point motion task. In the proposed *Time-indexed* learning from demonstration framework, the demonstrated trajectories with their corresponding time-index in multiple demonstrations are captured by a Gaussian mixture model, which is a probabilistic model that represents the data with finite Gaussian probability density functions. In the reproduction phase, in each *time* instance, the expected position is extracted from the learned Gaussian mixture model, using Gaussian mixture regression. Then using the introduced tangential-normal impedance controller the robotic system assists the patient to follow the trajectory at the demonstrated velocity of the therapist. In the other case, by proposing a Tangential-normal varying-impedance controller (TNVIC), the robotic manipulator not only follows the demonstrated motion but also mimics the therapist's interaction impedance during the assistive intervention. The feasibility

and efficacy of these frameworks are validated through experimens conducted involving a 2D play environment.

In the proposed *Position-indexed* learning from demonstration framework, by utilizing the modified non-parametric potential field function, the therapist's motion, impedance behavior, and interaction force (assistance/resistance) with the patient are encapsulated in each position time-independently, tangent and normal to the demonstrated trajectory. The potential field function is learned via a convex optimization algorithm. In the reproduction phase, the robot provides the patient with the same level of interaction force provided by the therapist in each position. Also, a position-indexed velocity field controller with a variable dissipative field actively regulates the level of patient's deviation from the velocity observed in the demonstration phase. The efficacy, advantages, and stability of the proposed framework are evaluated in three different experimental scenarios involving both position-based and impedance-based point-to-point motion tasks in a 2D play environment.

"The important thing is not to stop questioning. Curiosity has its own reason for existing. One cannot help but be in awe when he contemplates the mysteries of eternity, of life, of the marvelous structure of reality. It is enough if one tries merely to comprehend a little of this mystery every day."

- - Albert Einstein

Acknowledgements

First of all, I am thankful to my supervisors, Dr. Mahdi Tavakoli and Dr. Kim Adams, who have helped me through my M.Sc program in every aspect. Second, I would like to thank my examiners, Dr. Patrick Pilarski and Dr. Hamzeh Khazaei, for dedication to read my thesis and provide their insightful ideas. Then, I would like to express my gratitude and appreciation to my teachers, professors and friends who have helped me learn something new during all my years of education, fulfilling my thirst for knowledge.

Contents

List of Tables

List of Figures

List of Abbreviations

List of commonly used abbreviations

AAN	Assist As Needed
AT	Assistive Technologies
CP	Cerebral Palsy
DFR	Direct Force Reflection
DMP	Dynamic Motion Primitive
DOF	Degrees of Freedom
DS	Dynamic Systems
GMM	Gaussian Mixture Model
GMR	Gaussian Mixture Regression
HMM	Hidden Markov Model
LFD	Learning from Demonstration
PID	Proportional Integral Derivative
PDF	Probability Density Function
RLFD	Robot Learning from Demonstration
SEDS	Stable Estimator of Dynamical Systems
TNVIC	Tangential-Normal Varying Impedance Controller
TENS	Transcutaneous Electrical Nerve Stimulation

Chapter 1

Introduction

1.1 Motivation

Cerebral palsy (CP) is a group of non-progressive disorders in the central nervous system (CNS) that causes permanent posture and movement impairments in children within the first few years of their life [1, 2]. The most common symptoms of CP are stiffness of muscles, poor coordination in performing voluntary movement, weakness, tremor, delay in acquiring motor skills and difficulty in speaking or swallowing. CP is the dominant origin of motor disability in childhood, which affects 1.5 to more than 4 per 1,000 children around the world [3].

Although the symptoms of CP are permanent, they may be improved or compensated. Physical therapy and occupational therapy can help children with CP to ameliorate their motor function and live more independently by adjusting to their impairment [4]. However, based on a systematic review [5], these therapeutic approaches are mildly effective to rehabilitate CP symptoms. A more crucial concern for children with severe disability is missing the ability and opportunity to interact with real physical environments for object manipulation or general play [6]. This deprivation can hinder and adversely affect their natural, social, cognitive, perceptual and linguistic development [7].

Due to the cost and labor intensity of conventional hand-over-hand rehabilitative and assistive practices, there has been a growing interest in robotic systems to take over some labor. Robotic systems are consistent, untiring and robust in repetitive task executions. Also, with the sensory data and cutting-edge reinforcement learning, these systems can evaluate the patient's motor performance and accordingly provide the required assistance. In the near future, with the developments in machine learning assistive and rehabilitative robotic systems can become fully autonomous, making the role of the therapists supervisory in nature. However, machine learning algorithms need more development to progress to be reliable for fully autonomous assistive robotic systems considering the complexity of the tasks and the required safety guarantees for interaction with patients. Therefore, in this work we were motivated to develop semi-autonomous robotic-assistance frameworks that only require the short-term involvement of a helper to learn the required task-specific assistance and reproduce the same it in the therapist's absence safely. In this thesis, we propose and apply new learning from demonstration frameworks for robotic assistive systems that intuitively learn the therapist assistance by their physical intervention. So there is no need for manual programming of the robots which requires engineering and computer programming knowledge.

1.2 Organization of the Thesis

Chapter 2: This chapter provides a brief overview of the main concepts and backgrounds used in this thesis. First, the symptoms of CP and its negative impact on children's development is discussed. Then, assistive robotic controllers are introduced. In the next section, the Learning from Demonstration strategies which are developed for point-to-point motion tasks are reviewed. Finally, the background on Impedance-controller for human-robot interaction is presented in this chapter.

Chapter 3: In this chapter, we introduce a time-indexed learning from demonstration framework utilizing Gaussian mixture model and Gaussian mixture regression, together with a proposed tangential-normal impedance controller which regulates the interaction dynamics between therapist and patient in the robotic assistance phase. A teleoperation task-execution scenario for position-following game such as pick and place is considered in this section to validate the framework through experiments conducted involving a 2D play environment.

Chapter 4: This chapter extends the introduced framework in chapter 3 by proposing a tangential-normal varying-impedance controller (TNVIC). The TNVIC not only learns and reproduces the therapist's demonstrated motion but also mimics his/her interaction impedance behavior during the assistive intervention. The feasibility and efficacy of the proposed framework are evaluated by conducting an experiment in a 2D play environment, involving an adult (the author), with the symptoms of cerebral palsy being induced using transcutaneous electrical nerve stimulation.

Chapter 5: In this chapter we propose a position-indexed Learning from demonstration framework by use of potential field function which models the trajectory and interaction force observed in the therapist demonstration. Also, an active velocity field controller is proposed to regulate the patient's velocity while performing the task in robotic assistance phase. Finally, the efficacy, advantages, and stability of the proposed framework are evaluated in three different experimental scenarios involving both reaching motion and impedance-based tasks. Electrical nerve stimulation of an adult (the author) together with spring models are used to simulate the CP symptoms. Finally, **Chapter** 6 summarizes the research work and experiments and discuss the future direction of research.

1.3 Publications

Chapter 3 is published in International Journal of Intelligent Robotics and Applications, 2016. [8]

Chapter 4 is published in IEEE-RAS-EMBS International Conference on Rehabilitation Robotics, London, UK, July 2017. [9]

1.4 Contribution

In the proposed frameworks, a cooperative demonstration was introduced with both therapist and patient. In the cooperative demonstration, unlike [10, 11] where the therapist independently demonstrated the task, he/she interacts with the patient in task execution to sense and observe the patient's performance and accordingly provide the required assistance. In **Chapter 3** a master-slave teleoperation system is utilized with the master robot in the patient's hand and the slave robot performing the task in the environment. In the demonstration phase, a therapist holds the slave robot in the task environment to provide the required assistance for a few trials. However, in **Chapter 4** and **Chapter 5**, the therapist and patient both interact with the same robotic manipulator for the cooperative task demonstration.

Proposing a time-indexed motion leaning framework. In this framework unlike the previous Learning from demonstration frameworks for robotic assistance [10, 11], where a PID controller was used to regulate the interaction dynamics, in this thesis a time-varying impedance controller is employed which has been widely used in collaborative robotics. In **Chapter 3**, a **tangential-normal impedance controller** is proposed. This time-varying controller, with its constant virtual impedance models, rotates towards the tangential direction to independently control the interaction dynamic, tangent and normal to a trajectory that is produced by Gaussian mixture regression. In **Chapter 4**, this controller is extended to the proposed **tangential-normal varying**

impedance controller (TNVIC). Using the TNVIC, the virtual impedance models not only rotate to tangential-normal coordinates but also, change in magnitude about the desired trajectory (which dictates the level of assistance provided to the patient) in inverse proportion to the trial-to-trial variation of the demonstrated trajectories. Thus, the lower the variability in demonstrations at a given time, the more assistance is required to be provided to the patient, and the higher the impedance parameters (spring-damper) to restrict deviation from the desired trajectory.

The potential field function learning from demonstration algorithm that was developed in [12], with its optimization goal and controller are modified and adapted to the context of robotic assistance in **Chapter 5** to generate position-indexed motion that not only follows the same *trajectory* but also follows the same *interaction force* profile experienced during the demonstration. Then, in the therapist's absence, the robot not only provides the patient with the same assistance he/she received during the task demonstration, but also with a proposed performance-based and stable active **velocity field controller** that assists/resists the patients, if they are following the trajectory slower/faster than the demonstrated velocity. Additionally, a tank-based passivity controller [13] is adopted to ensure the stability of the overall system, having the active velocity controller.

In short the main contributions of this thesis are:

- Learning therapist's assistance from cooperative therapist-patient demonstration.

- Mapping the trajectory following task into principal tangential-normal coordinates in both learning and robotic assistance phases in the proposed time-indexed and position-indexed frameworks.

- Proposing a tangential-normal varying impedance controller (TNVIC) to regulate the interaction dynamic in the proposed time-indexed motion

learning framework.

- Modifying the potential field function proposed in [12] to learn the trajectory and interaction force from the therapist-patient cooperative demonstration and reproduce the same assistace time independently (i.e., position-indexed).

- Augmenting a proposed demonstrated velocity field with a passive velocity field controller to the learned potential field function to regulate the patient's velocity along the trajectory.

Chapter 2

Background & Related Work

2.1 Assistive Robotic Systems

In this section. First, the main symptoms of CP are introduced. Then necessity of play and object manipulation, and how the robotic systems can assist children with CP to perform the act of playing independently is presented. Finally, the current algorithms for robotic assistance for point-to-point motion tasks are investigated.

2.1.1 Symptoms of CP

Cerebral palsy (CP) corresponds to a class of non-progressive impairments in the central nervous system caused by brain and neurological damage in early stages of children life [1, 2]. CP is mainly categorized into spastic, ataxic and dyskinetic types based on the primary symptoms and part of the central nervous system which is mainly damaged. The most common type of CP is spastic CP which is caused by damage to the motor cortex. The motor cortex initiates and controls voluntary movements, therefore any damage to the motor cortex can inhibit the individuals with CP to start and control movements. This results in stiffness, tightness (spasticity) and incoordination in muscles.

Ataxic CP is caused by damage to the cerebellum in the brain. The cerebellum receives information from the sensory systems and then regulates motor movements accordingly. Therefore individuals with ataxic CP have problem in balance and coordination motions and demonstrate tremor and shakiness in their movements. Finally, the dyskinetic CP is due to the damage to basal ganglia, which is the balance control system in the brain. People with dyskinetic CP demonstrate involuntary and repetitive muscle tone.

People with CP can have one or several of the symptoms associated with the introduced CP categories. CP can seriously decrease one's ability for active motion control, object manipulation and environmental exploration.

2.1.2 Play and Object Manipulation in Children with CP

Play and object manipulation contribute to children's physical, cognitive and social development[14]. The theory of cognitive development that was proposed in [15], states that in the first two years of life, functional play contributes to the development of motor reflexes, simple motor actions, imitation of behaviors, exploration of the environment and object manipulation. Therefore, play is associated with the development of complex cognitive and motor skills [16].

Children's environmental exploration as an ongoing cycle of action, perception, and cognition was introduced by Gibson's theory of development [6]. In children with CP, this cycle is interrupted due to physical impairments that can restrict children's exploratory behavior in the environment and postpone or halt their perceptual and cognitive skills [6]. Assistive technologies (AT) have been used to compensate for these disabilities and assist children with CP to do the act of playing, object manipulation and further exploration of their environment [17, 18].

2.1.3 Assist-as-Needed Robotic Systems

Robotic systems as an assistive technology have been advancing in the recent years. Robots can utilized to either build function for children to independently engage in activities (e.g., rehabilitation robots), or compensate for their function (e.g., assistive robots). In assistive robotic systems, one focus in the literature has been to provide assistance in an as needed paradigm (also called assist-as-needed (AAN)). Robotic-assistance with AAN not only motivates children's active participation in the task but also provokes motor action and contribution in task execution. By providing excessive assistance, the users instinctively decrease their effort and let the robotic system complete the task, on the other hand, by giving lower than the required assistance, the users may not be able to complete the task, which decreases their confidence and contribution in task execution [19].

Several control frameworks have been suggested for ANN including impedance control [20]. Impedance control is most beneficial in applications with human-robot interaction as the robot controller imposes a virtual mass-spring-damper behavior in the interaction dynamic [21, 22]. This provides an adjustable flexibility required for interactive tasks. A virtual impedance model connecting the patient's hand to a moving target along the predefined trajectory was defined in [23, 24]. Thus, the patient does not feel any assistive force unless he/she deviates from the target trajectory. A force tunnel produced by a virtual impedance model that restricts the patient in directions orthogonal to his/her movement direction was developed in [25]. In [26], a time limit was also proposed for patients to finish a task by defining a moving virtual wall that would push and assist the patient in case they were moving slower than expected. The authors in [27] used position, force, and impedance control to provide a virtual-tunnel model for guidance in the tangential and virtual-wall-like restriction in the normal directions of the trajectory.

The major drawback of the stated assist-as-needed frameworks is the re-

quirement for manual robot programming in order to plan the desired trajectory which requires advanced coding and engineering skills that are not necessarily available in settings such as clinics and patient's homes. Even having the required skills, it would be a non-intuitive and arduous struggle to mathematically model these task-dependent assistance models every time the task changes, especially in motions that involve high degrees of freedom (e.g., if the locations of object picking and placing changes). As a result, a robot learning from demonstration (RLfD) technique was utilized for rehabilitation applications in [10, 11].

2.2 Learning from Demonstration

Even though robotic technologies and artificial intelligence have developed significantly, still they cannot plan the motions, as well as a human does. Most of the advanced robotic systems are still programmed manually for most of their functions. Specifically in assistive and therapeutic systems, due to the complexity of the task and required safety considerations, it is not yet feasible to rely completely on artificial intelligence. Therefore, semi-autonomous robot learning from demonstration (RLfD) is the focus in this paper. In this framework, a short duration of therapist interaction with the patient (through a robotic medium) is enough to learn the task-specific assistance provided by the therapist to the patient and subsequently administer the same assistance to the patient robotically in the therapist's absence.

RLDF (also called robot imitation learning, robot programming by demonstration) is founded based on intuitive principles used by humans to learn new tasks in their everyday lives. Before performing any task for the first time, we observe it done by an expert, and then we try to imitate the same performance in the task execution. RLfD started in the early 80s [28] and has developed over the years as an intuitive, fast and user-friendly programming

procedure for various applications like helicopter control [29], grabbing flying objects [30], teaching to play golf [31], etc. In this thesis, robotic point-to-point motion learning has been considered as the main focus. Point-to-point motion learning is the building block for complex trajectories used in assistive and therapeutic systems. In the following section, time-indexed and position-indexed approaches for learning from demonstration will be discussed briefly.

2.2.1 Time-Indexed Motion Leaning

Time-indexing is a classical approach to trajectory planning and encoding. In [32, 33, 34] spline smoothing techniques together with averaging of demonstrated trajectories were used to deal with variability across demonstrated trajectories. Although this method is fast and straightforward, it is highly task-dependent as a heuristic is needed to segment the trajectories. Therefore this approach is inefficient in capturing non-linear trajectories accurately.

An alternative probabilistic approach is using Hidden Markov Model (HMM) to capture the temporal-spatial variability of the demonstrated trajectories with a sequence of hidden states [35, 36]. The HMM model has been extensively used in speech and gesture recognition systems as it can capture the sequential behavior of a demonstrated signal with temporal dissimilarity [37]. One of the disadvantages of the HMM is that it cannot reproduce a smooth trajectory required for human-robot interactive tasks, but instead a discrete and stepwise one. A candidate solution is averaging over many stochastic samples. This solution can produce a smooth trajectory with the cost of under-fitting the trajectory and missing the trajectory information, which can reduce the accuracy. To solve this problem, Calinon [38] integrated the HMM with Gaussian Mixture Model (GMM) and Gaussian Mixture Regression (GMR) to model and reproduce a smooth trajectory. However, it still required a lot of demonstration data to accurately capture the state transition model in HMM, which makes it inappropriate for the application focused on this thesis.

Using Gaussian Mixture Models (GMM) to model a number of trajectories with its time index through a weighed average of several Gaussian probability density functions and then Gaussian Mixture Regression (GMR) as a regression technique to reproduce the generalized smooth trajectory in each time index was first proposed in [39] and ever since has been extensively used [39, 40, 41]. The GMM fits the dataset via the Expectation-Maximization (EM) algorithm [42]. Some of the advantages of the GMM/GMR approach are: 1) Few demonstrations are required for effective learning of motion and smooth trajectory reproduction; 2) Correlation between motion states and the variability of these states along each dimension are captured statistically; and 3) The reproduction phase is computationally cheap and efficient for real-time implementation [43]. However, similar to other time-indexed approaches, the explicit dependence on time to reproduce the generalized trajectory makes this approach open-loop and unable in facing temporal perturbations.

2.2.2 Position-Indexed Motion Leaning

In this thesis, a point-to-point motion is considered as the target application, therefore we classify any RLfD technique which is not using time-index to reproduce the motion as position-indexed motion learning algorithms. Movement primitives are asymptotically stable differential equations that represent a generalized trajectory. This approach for RLfD is closed-loop as the learned differential equation represents the dynamics of the motion which can face unforeseen spatial and temporal perturbations (this technique is also called Dynamic system-based RLfD).

One of the non-probabilistic dynamic system-based approaches for motion learning is dynamic motion primitives (DMP), in which a non-linear asymptotically stable dynamic system is estimated for reaching to the equilibrium point, through a single demonstration. However, this approach is nonprobabilistic and a task-dependent heuristic is required as a phase variable to enforce the con-

vergence [44]. The other approach is Stable Estimator of Dynamical Systems (SEDS) which was proposed in [45], and has been used for various applications since its introduction [29, 30, 31]. In SEDS the demonstrated position-velocity trajectories are captured using the GMM with a modified EM algorithm to ensure the asymptotic stability of the dynamic systems. Then using GMR, the generalized trajectory is produced by position as an input and desired velocity as an output of the SEDS, which should be followed by the robotic manipulator. Most of the research in dynamic systems considered free space motions and thus do not consider robot-environment interaction exists in assistive robotic systems. Recently some work has been done to use SDES on robotic interaction and providing stability of the interaction dynamics [46].

Potential field motion planning was introduced in [47]. In this approach, a global potential function models the workspace and the robot is considered as a particle which is influenced by the gradient (i.e., force) of this field. The Global potential function is produced by the sum of several attracting points (destination) and repelling points (obstacles). There are various algorithms to place these attracting/repelling points in the task space to have reachable (not asymptotically stable) destinations. Navigation function was first introduced in [48], this technique was an approach to form a field which is free from local minima along the trajectory. The harmonic potential is a navigation function approach that replicates the dynamics of some physical processes such as heat transfer or fluid flow. This approach proves the asymptotic stability of the potential field, however, the navigation function is restricted to simple environments with specific obstacle shapes. Approximate methods based on discretized space overcome this limitation but at the cost of being computationally more expensive [49].

A novel technique for motion leaning from demonstration, based on the Potential field approach was recently proposed in [12]. In this work, several attracting points are assigned to the sampled demonstrated trajectory, then

using a convex optimization algorithm, the bias potential parameter for the sampled points are learned to dictate a tangential force along the trajectory to have a reachable destination. Also, a damping parameter is assigned to each attracting point via another convex optimization algorithm to replicate the same velocity behavior as-demonstrated. Some of the advantages of this technique are: 1) It is time-independent and robust to temporal and spatial perturbation; 2) A single demonstration is sufficient to learn the trajectory; 3) The potential field strategy for trajectory planning is passive and stable in interaction with passive environments; 4) The potential field function cannot only encode the demonstrated trajectory, but also the force profile which makes this approach suitable for robotic assistance tasks involving human-robot interactions; 5) Multiple trajectories can be encoded into a single potential field function in the task space.

2.3 Impedance Control

Impedance control [21] has been widely used in collaborative robotics to regulate the interaction between the human and the robotic manipulator. In this controller, the position-force relationship is dictated by an interaction dynamics instead of solely tracking the position/force trajectories which can be prone to failure in tasks with human-robot interaction. The virtual interaction impedance model (usually a mass-spring-damper model) is either constant or variable. Variable impedance controllers provide higher performance by adapting the interaction properties while cooperatively accomplishing a task such as following a given path, for instance by making it less compliant where more accuracy is required [50, 51].

Various strategies have been introduced for varying impedance control in recent years. [52] optimized the interaction performance with reinforcement learning, using the human motor control and equilibrium point models. [53]

employed Game Theory in the human-robot Two-Agent system. The developed an adaptation law to adjust the impedance controller parameters based on the human's intention to lead or follow. [54] introduced an optimal control approach to regulate the time-varying stiffness profiles.

A learning from demonstration approach was employed in [55] to alter the stiffness parameters in task space inversely proportional to the observed covariance in the demonstrated trajectories. Therefore, less variability in the demonstration will result in a larger impedance parameter (i.e., more accuracy) in the reproduction phase. In [56] an adaptive controller was proposed to regulate the interaction dynamic for human-like reproduction of a cooperative task which is learned through demonstration.

Although variable impedance control has been extensively used in interactive robotic systems, few works have considered the stability of the interaction dynamics. In [13], an energy-tank passivity controller was proposed which stores the passive (i.e., damped) interaction energy in a virtual state (called energy tank), and uses this energy to implement impedance variations. In [57], they introduced a state-independent energy-tank passivity controller with increased performance and reliability. The same energy-tank approach was used in [46] for tracking the velocity field produced by Dynamic Systems. [50] developed an adaptive approach to guarantee the stability of their variable impedance controller.

Chapter 3

Learning from Telecooperative Demonstration Using Time-indexed Motion Learning

In this chapter, the goal is to propose a AAN framework for a two-dimensional (2D) position-following pick-and-place task via a teleoperation system. In this framework, for the first time, a tangential-normal ($T-N$) impedance controller is utilized together with a GMM/GMR learning from demonstration (LfD) technique. The tangential-normal impedance controller acts as an attractor around the learned trajectory and provides robustness to spatial perturbation. The proposed scheme with its demonstration and robotic assistance phases is sketched in Fig.3.1. In the first phase, the therapist provides assistance as needed and cooperates with the child to perform the task a few times. In this phase, the therapist assistance is modeled by a GMM and the average trajectory demonstrated by the therapist is approximated using GMR. In the second phase, tangential-normal impedance controller is proposed, so that the master robot handled by the child assists the child to follow the average demonstrated trajectory in the tangential direction and resists the child's motion in the normal direction. In both the tangential and normal directions, the level of

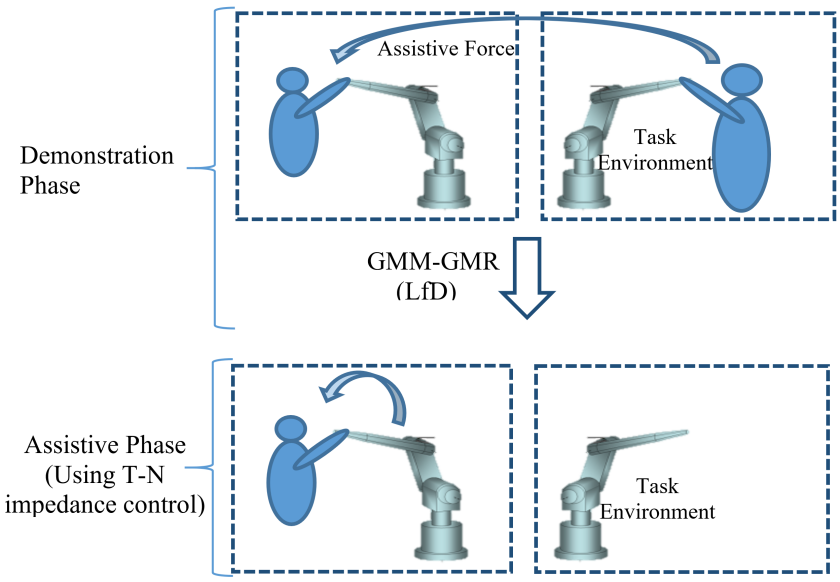

Figure 3.1: The schematic of proposed robotic assistance framework including demonstration and assistive phases.

assistance/resistance can be adjusted by tuning the time-invariant parameters of the impedance models.

3.1 Dynamics of Master-Slave Teleoperation System

The nonlinear dynamics of the multi-DoF master and slave robots side in the Cartesian coordinates are

$$M_{x,m}(q_m)\ddot{x}_m + C_{x,m}(q_m, \dot{q}_m)\dot{x}_m + G(q_m) + F_{x,m}(\dot{q}_m) = F_m + F_{ext,m} \tag{3.1}$$

$$M_{x,s}(q_s)\ddot{x}_s + C_{x,s}(q_s, \dot{q}_s)\dot{x}_s + G(q_s) + F_{x,s}(\dot{q}_s) = F_s + F_{ext,s} \tag{3.2}$$

where q_m and $q_s \in R^{n\times 1}$ are joint angles. x_m and $x_s \in R^{n\times 1}$ are, respectively, the positions of the master and slave end-effectors in the Cartesian coordinates. $M_{x,m}(q_m)$ and $M_{x,s}(q_s) \in R^{n\times n}$ are inertia matrices, $C_{x,m}(q_m, \dot{q}_m)$ and $C_{x,s}(q_s, \dot{q}_s) \in R^{n\times n}$ contain Coriolis and Centrifugal terms, $G(q_m)$ and

$G(q_s) \in R^{n\times 1}$ vectors represent position-dependent forces such as gravity, $F_{x,m}(\dot{q}_m)$ and $F_{x,s}(\dot{q}_s) \in R^{n\times 1}$ are the friction forces, F_m and $F_s \in R^{n\times 1}$ are the control signals for the robot's actuators and $F_{ext,m}$ and $F_{ext,s} \in R^{n\times 1}$ are the external forces exerting on robot's end-effector. In this chapter, the master and slave robots are respectively in contact with child and the therapist. Thus, the external forces are

$$F_{ext,m} = F_{ch} \tag{3.3}$$

$$F_{ext,s} = -F_{th} - F_e \tag{3.4}$$

where $F_{ch} \in R^{n\times 1}$ is the child's force exerted on the master robot, and $F_{th} \in R^{n\times 1}$ and $F_e \in R^{n\times 1}$ are, respectively, the therapist's and the task environment's forces applied to the slave robot. Note that as the slave interacts with the task environment, the therapist pulls/pushes the slave in order to assist the child in terms of completing the task. It is assumed that the slave robot is either inherently back-drivable or is properly impedance controlled to follow externally-imposed motions.

3.2 Demonstration Phase

In this work, a pick and place game is chosen as the position-following task for the child. The child interacting with the master robot manipulates the slave robot to perform a task in the remote environment through a teleoperation system. Meanwhile, the therapist interacts with the slave robot in order to assist and modify the child's movements, considering the child's unique motion and posture characteristics. The position trajectory data from multiple task trials is then saved to be encoded using GMM and GMR.

Transparency in the teleoperation system is provided when the perfect position and force tracking are simultaneously achieved in the master-slave robotic setup. In order to provide transparency, the Direct force reflection (DFR) archi-

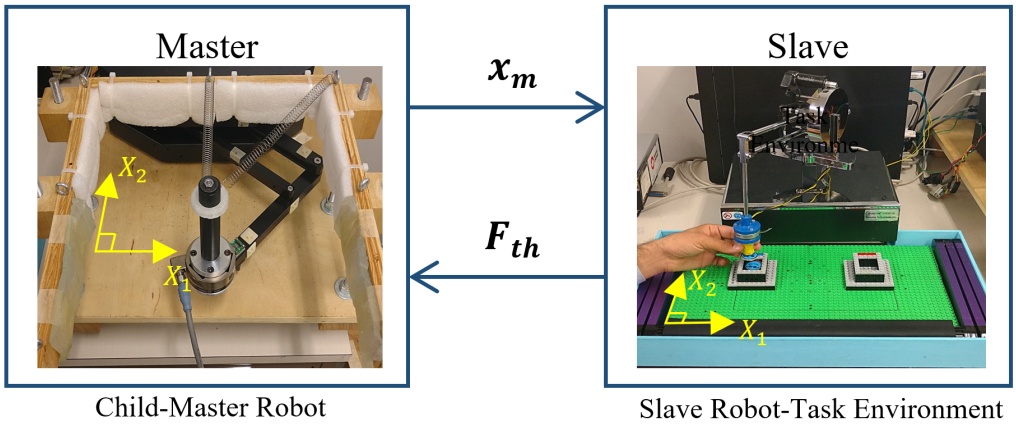

Figure 3.2: Direct force reflection (DFR) strategy for the cooperation of the child and therapist in the demonstration phase.

tecture is employed [8]. In this control method, the master position trajectory is transmitted to and tracked by the slave robot. Also, the slave-therapist interaction force is reflected back to the master robot to be fed back to the child, as schematically shown in Fig.3.2.

The obtained data from a cooperative demonstration of the pick-and-place task through a transparent teleoperation system is constructed by 2-dimensional position vector ($S^p \in R^2$) and a 1-dimensional time variable ($S^t \in R$). The size of the total demonstration dataset is determined by the number of sampled data in each trial (N), multiplied by the total number of demonstration trials (M). So the resulting $M.N$ samples form the total database of

$$D = \begin{bmatrix} S^p_{1,1} & S^p_{1,2} & \dots & S^p_{m,n} & \dots S^p_{M,N} \\ S^t_{1,1} & S^t_{1,2} & \dots & S^t_{m,n} & \dots S^t_{M,N} \end{bmatrix} \tag{3.5}$$

In (3.5), m and n subscripts indicate the n^{th} sample of a signal in the m^{th} demonstration. The Gaussian mixture model (GMM) will be used to statistically model the demonstration database ($D \in R^{3\times M.N}$). The GMM is a probabilistic model that represents the data by a mixture of finite Gaussian

probability density functions (PDF) [55] as

$$f(S^p, S^t; \theta_i) = \sum_{i=1}^{K} h_i \mathcal{N}(S^p, S^t; \mu_i, \Sigma_i) \tag{3.6}$$

$$\mathcal{N}(S^p, S^t; \mu_i, \Sigma_i) = \frac{1}{\sqrt{2\pi^3 |\Sigma_i|}} e^{-\frac{1}{2}\left(([S^P; S^t]-\mu_i)^T \Sigma_i^{-1} ([S^P; S^t]-\mu_i)\right)} \tag{3.7}$$

$$\mu_i = \begin{bmatrix} \mu_i^p \\ \mu_i^t \end{bmatrix}, \Sigma_i = \begin{bmatrix} \Sigma_i^p & \Sigma_i^{p,t} \\ \Sigma_i^{t,p} & \Sigma_i^t \end{bmatrix} \tag{3.8}$$

where $\mathcal{N}$ represents the joint 3-dimensional normal probability density function (PDF). K is the number of Gaussian mixture models. $\theta_i = \{h_i \in R^3, \mu_i \in R^3, \Sigma_i \in R^{3\times 3}\}$, denotes the prior weight, the mean value and the covariance matrix for each of Gaussian mixture components, respectively. The Expectation-Maximization (EM) algorithm [42] is used to iteratively train the GMM model (θ_i) on total dataset (D), which is subject to the following constraint:

$$\sum_{i=1}^{K} h_i = 1, \ 0 < h_i < 1. \tag{3.9}$$

The obtained GMM should be customized to be utilized for the trajectory following task of pick and place considered in this chapter. The average demonstrated position in a given time is needed for feeding the controller later in robotic-assistance phase. This conditional probability is achieved using Gaussian mixture regression (GMR) [10] as

$$f(S^p | S^t; \theta_i) = \sum_{i=1}^{K} \omega_i \mathcal{N}(S^p; \widehat{\mu_i^P}, \widehat{\Sigma_i^P}) \tag{3.10}$$

$$\mathcal{N}(S^p; \widehat{\mu_i^P}, \widehat{\Sigma_i^P}) = \frac{1}{\sqrt{2\pi^2 |\widehat{\Sigma_i^P}|}} e^{-\frac{1}{2}\left(([S^P; S^t]-\widehat{\mu_i^P})^T \widehat{\Sigma_i^P}^{-1} ([S^P; S^t]-\widehat{\mu_i^P})\right)} \tag{3.11}$$

where $\widehat{\mu_i}$,$\widehat{\Sigma}_i$ are the expected mean and covariance matrix of the i^{th} condi-

tional probability as

$$\widehat{\mu_i^P} = \mu_i^P + \Sigma_i^{P,t}(\Sigma_i^t)^{-1}(S^t - \mu_i^t) \in R^2 \tag{3.12}$$

$$\widehat{\Sigma_i^P} = \Sigma_i^t + \Sigma_i^{P,t}(\Sigma_i^t)^{-1}\Sigma_i^{t,P} \in R^{2\times 2} \tag{3.13}$$

The probability that S^t is in the i^{th} Gaussian distribution component (ω_i) is

$$\omega_i = P(i|S^t = t;\theta_i) = \frac{h_i\mathcal{N}(S^t;\mu_i^t,\Sigma_i^t)}{\sum_{i=1}^K h_i\mathcal{N}(S^t;\mu_i^t,\Sigma_i^t)} \tag{3.14}$$

now, the single Gaussian distribution of the conditional expectation of S^p, given $S^t = t$, can be approximated as

$$f(S^p|S^t;\theta_i) \approx \mathcal{N}(S^p;\widehat{\mu^P},\widehat{\Sigma^P}) \tag{3.15}$$

$$\widehat{\mu^P} = \sum_{i=1}^K \omega_i\widehat{\mu_i^P},\ \widehat{\Sigma^P} = \sum_{i=1}^K \omega_i^2\widehat{\Sigma_i^P} \tag{3.16}$$

$\widehat{\mu^P}$ is the average position demonstrated during the cooperation of the child and the therapist at each time. Considering the orthonormal 2-dimensional Cartesian $X_1 - X_2$ coordinate, these vectors can be rewritten as

$$\widehat{\mu^P} = \begin{bmatrix} \widehat{\mu_t^{X_1}} \\ \widehat{\mu_t^{X_2}} \end{bmatrix} \tag{3.17}$$

where the subscript t, represents the time in which the $\widehat{\mu^P}$ is achieved. $\widehat{\mu_t^{X_1}} \in R$ and $\widehat{\mu_t^{X_2}} \in R$ denote the projection of $\widehat{\mu^P}$ along the X_1 and X_2 Cartesian coordinates, respectively. In summary, the demonstrated trajectory is modeled in the $X_1 - X_2 - t$ space via the GMM/GMR algorithms. For a given time, the expected 2-dimensional $X_1 - X_2$ statistical model for the demonstrated position is approximated via (3.15)-(3.16). Then, the expected average position in that time is calculated in each of X_1 and X_2 using (3.17), which will be later utilized

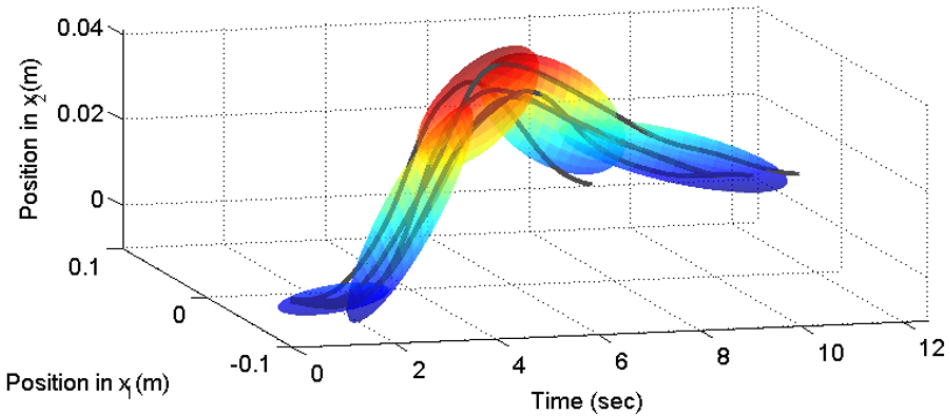

(a)

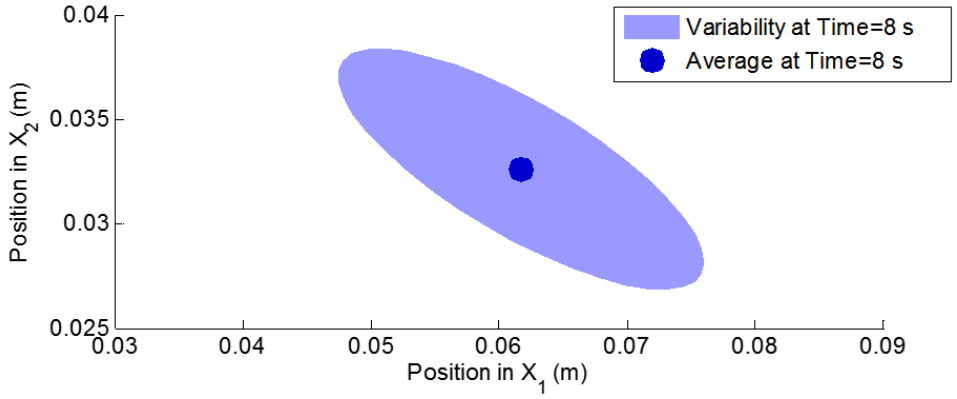

(b)

Figure 3.3: LfD process: (a) The 3-dimensional Gaussian Mixture Models (GMM) capture the 3-dimensional $X_1 - X_2 - t$ dataset (D), and (b) The 2-dimentional $X_1 - X_2$ Gaussian probability density function (pdf) in a given time ($t = 8s$) resulting from GMR. Variability is shown as area inside 3 at each direction.(σ is the Gaussian variance).

in our proposed controller (Fig.3.3). In Fig.3.3, an example of the GMM/GMR process is shown. Fig. 3.3(a), displays five 3-dimensional Gaussian models that captured the demonstrated trajectories in $X_1 - X_2 - t$ space. Fig.3.3(b), depicts a 2-dimensional Gaussian probability density function (PDF) resulting from GMR in a given time ($t = 8s$). Using GMR, the average and variability of position in $X_1 - X_2$ subspace can be approximated by a 2-dimentional Gaussian PDF at any time instance. The time ($t = 8s$) in Fig.3.3(b) was chosen randomly to provide an example of GMR output.

3.3 Robotic Assistance Phase

In this section, the aim is to propose a framework which utilizes the learned average demonstrated position from the previous section so that the robot can take over the therapist's role and autonomously assist the child to follow the desired point-to-point trajectory in the pick and place task. In this framework, two desired virtual impedance models are defined in the master robot. These impedance models control the interaction dynamics of the master robot around the average demonstrated trajectory ($\widehat{\mu^P}$) in tangential and normal directions. Then, the slave robot, which is in contact with task environment, follows the master position through a unilateral teleportation system so that the child can perform the task on his/her own.

3.3.1 Master Robot's Tangential-Normal Impedance Controller

The objective is to design a framework so that the master robot imitates the therapist's demonstrated performance and provides assistance to the child to follow the average demonstrated position trajectory from point A to point B. Depending on the task and the child, it may be desirable for the therapist to provide different levels of assistance/resistance in directions that are tangential/normal to the trajectory's direction. For this purpose, a tangential-normal coordinate $T-N$ in each time is defined by setting the average demonstrated position at the current time ($\widehat{\mu^P}$) as the origin of the new $T-N$ coordinate. The rotation of the $T-N$ frame can be computed via differentiating the average position trajectory ($\widehat{\mu^P}$) as

$$\theta_{T,t} = Arctan\Big(\Big(\widehat{\mu_t^{X_2}} - \widehat{\mu_{t-\Delta t}^{X_2}}\Big) \Big/ \Big(\widehat{\mu_t^{X_1}} - \widehat{\mu_{t-\Delta t}^{X_1}}\Big)\Big) \tag{3.18}$$

$$R_t = \begin{bmatrix} cos(\theta_{T,t}) & sin(\theta_{T,t}) \\ -sin(\theta_{T,t}) & cos(\theta_{T,t}) \end{bmatrix} \tag{3.19}$$

$$\widehat{H_t} = \begin{bmatrix} R^t & & -\widehat{\mu_t^{X_1}} \\ & & -\widehat{\mu_t^{X_2}} \\ 0 & 0 & 1 \end{bmatrix} \tag{3.20}$$

where $\theta_{T,t} \in [-\pi \quad \pi]$ denotes the angle between the $T-N$ and $X_1 - X_2$ Cartesian coordinates in a given time ($S^t = t$), calculated by four-quadrant inverse tangent. Δt represents the sampling period. R_t and H_t express the rotation and homogeneous transformation matrix [58], which maps each interaction force and position vector from $X_1 - X_2$ to $T - N$ coordinate at a given time (t) as

$$\begin{bmatrix} F_T \\ F_N \end{bmatrix} = R_t \begin{bmatrix} F_{X_1} \\ F_{X_2} \end{bmatrix} \tag{3.21}$$

$$\begin{bmatrix} x_T \\ x_N \\ 1 \end{bmatrix} = H_t \begin{bmatrix} x_{X_1} \\ x_{X_2} \\ 1 \end{bmatrix} \tag{3.22}$$

In the next step, at a given time, two virtual impedance model are defined in directions tangential and normal to the average demonstrated trajectory. This models indicates the desired linear interaction dynamic between the master robot and the target trajectory in $T - N$ Cartesian space (Fig.3.4) as

$$m_T \ddot{\widetilde{x}}_T + c_T \dot{\widetilde{x}}_T + k_T \widetilde{x}_T = -F_{ch,T} \tag{3.23}$$

$$m_N \ddot{\widetilde{x}}_N + c_N \dot{\widetilde{x}}_N + k_N \widetilde{x}_N = -F_{ch,N} \tag{3.24}$$

where $\{m_T, c_T, k_T\} \in R^+$ and $\{m_N, c_N, k_N\} \in R^+$ refer to the desired virtual mass, damping and stiffness parameters in the tangential and normal directions,

respectively. $\widetilde{x}_T = x_{des,T} - x_{dem,T}$ and $\widetilde{x}_N = x_{des,N} - x_{dem,N}$ indicate the difference between the desired robot position $\{x_{des,T}, x_{des,N}\} \in R$ and the demonstrated trajectory at a given time $\{x_{dem,T}, x_{dem,N}\} \in R$ as transformed to the $T-N$ frame, respectively. $F_{ch,T}$ and $F_{ch,N} \in R$ denote the interaction force between the child and the master robot in $T-N$ coordinates, which are found as

$$\begin{bmatrix} F_{ch,T} \\ F_{ch,N} \end{bmatrix} = R_t \begin{bmatrix} F_{ch,X_1} \\ F_{ch,X_2} \end{bmatrix} \tag{3.25}$$

$$\begin{bmatrix} x_{dem,T} \\ x_{dem,N} \\ 1 \end{bmatrix} = H_t \begin{bmatrix} \widehat{\mu_t^{X_1}} \\ \widehat{\mu_t^{X_2}} \\ 1 \end{bmatrix} = \begin{bmatrix} 0 \\ 0 \\ 1 \end{bmatrix} \in R^2 \tag{3.26}$$

Equivalently, $\dot{\widetilde{x}}_T$, $\ddot{\widetilde{x}}_T$, $\dot{\widetilde{x}}_N$, $\ddot{\widetilde{x}}_N$ are

$$\begin{bmatrix} \dot{\widetilde{x}}_T \\ \dot{\widetilde{x}}_N \end{bmatrix} = R_t \begin{bmatrix} \dot{x}_{des,T} \\ \dot{x}_{des,N} \end{bmatrix} \in R^2 \tag{3.27}$$

$$\begin{bmatrix} \ddot{\widetilde{x}}_T \\ \ddot{\widetilde{x}}_N \end{bmatrix} = R_t \begin{bmatrix} \ddot{x}_{des,T} \\ \ddot{x}_{des,N} \end{bmatrix} \in R^2 \tag{3.28}$$

In Fig.3.4, the red and green orthogonal axes represent the $T-N$ and X_1-X_2 Cartesian coordinates respectively. The $T-N$ origin is on the average demonstrated trajectory at a given time which acts as a moving target in this controller ($\widehat{\mu^P}$). In the first step, the child's applied force on the master (F_{ch}) is projected along $T-N$ coordinates by (R_t) and then exerted to their corresponding virtual mass-damper-spring models that are connected to the virtual moving target ($\widehat{\mu^P}$). These forces cause a deviation with respect to the moving target and find the desired master robot position in each of tangential/normal directions ($x_{des,T}$,$x_{des,N}$), so that the master robot get connected to the desired virtual moving target via virtual impedance models. These desired positions

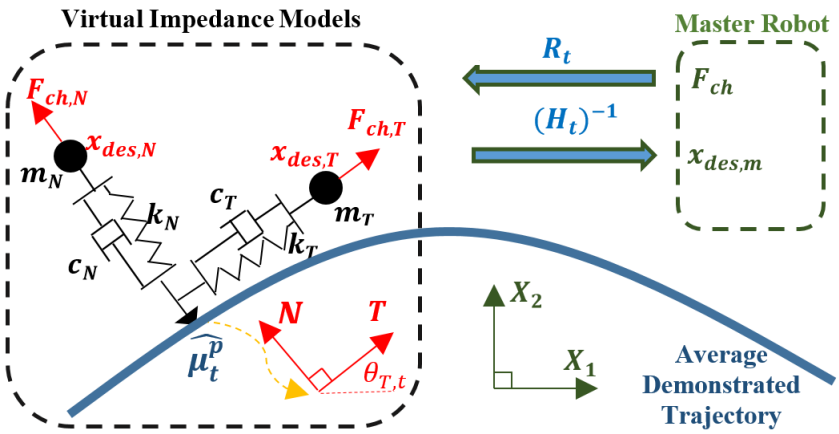

Figure 3.4: The proposed virtual tangential-normal impedance controller.

are then map back to $X_1 - X_2$ coordinate (3.29) for the master robot to be followed. Accordingly, the child feels as if connected to a moving target ($\widehat{\mu^P}$) via virtual mass-damper-spring impedance models in each of tangential and normal directions Fig.3.4. Therefore, the master robot not only follows the average demonstrated position, but also provides an adjustable level of freedom for the child to deviate from this trajectory in each direction. The larger the desired impedance parameters, the less the child's freedom to deviate from the expected trajectory.

$$\begin{bmatrix} x_{des,X_1} \\ x_{des,X_2} \\ 1 \end{bmatrix} = H_t^{-1} \begin{bmatrix} x_{des,x_T} \\ x_{des,x_N} \\ 1 \end{bmatrix} \tag{3.29}$$

3.3.2 Unilateral Teleoperation Control

A unilateral teleoperation system Fig.3.5 is used, where the master position is transmitted to the slave side to be used as the desired position for slave:

$$x_{des,s} = x_m \tag{3.30}$$

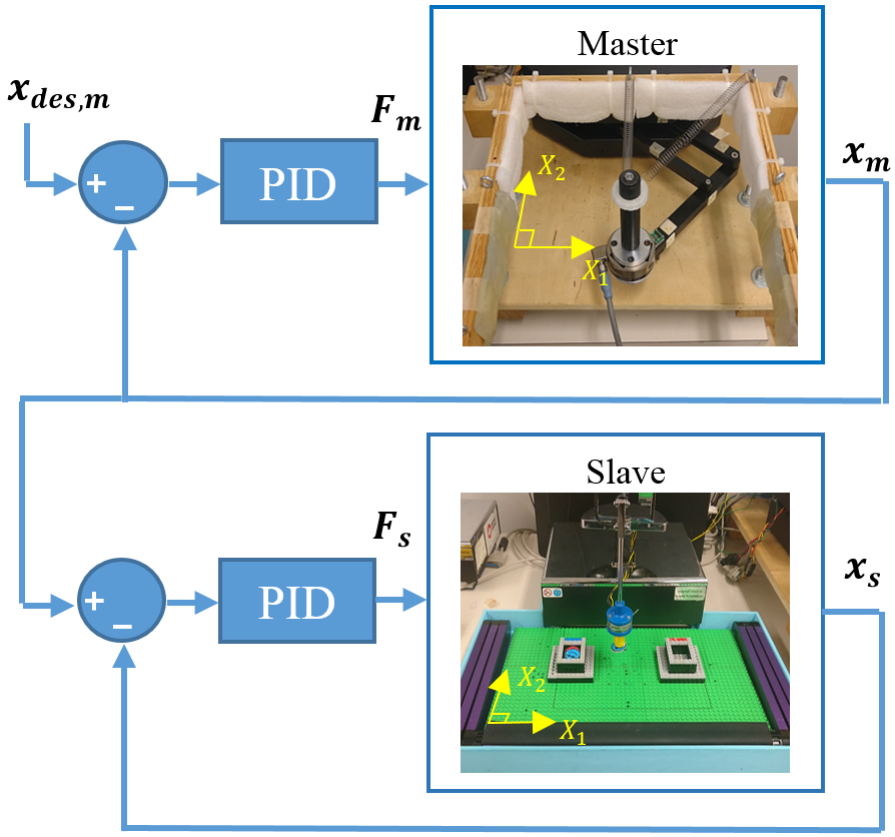

Figure 3.5: Unilateral teleoperation system. The slave robot (in play environment) follows the position of master robot (child) that is connected to the virtual $T - N$ impedance models.

Here, $x_{des,s} \in R^2$ denotes the desired position for slave robot. And, $x_m \in R^2$ expresses the master robot position transmitted from master side. A PID controller is utilized, so that the master and slave robots follow their desired positions.

3.4 Experiments and Discussion

The proposed AAN framework using LfD was experimentally tested using a Quanser Rehab robot (Quanser Consulting Inc., Markham, Canada) as the master (Fig.3.6(a)) and a Phantom Premium robot (Geomagic Inc., Wilmington, USA) as the slave (Fig.3.6(a)). Both of the therapist demonstration

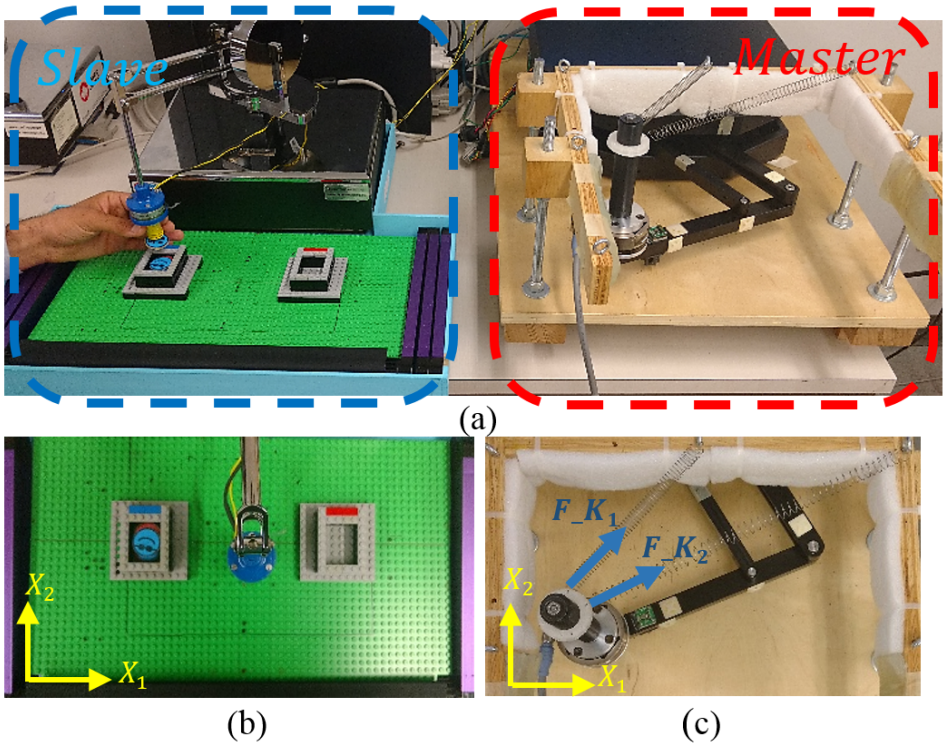

Figure 3.6: The experimental set up: (a) Quanser Rehab robot (Master) and Phantom Premium robot (Slave) in the teleoperation system, (b) the game environment, where the task was to pick tokens from box A and place them in box B, and (c) the spring array (K_1,K_2), modeled the child with disability in the master robot side.

and robotic assistance phases were implemented with a sampling time of 1 msec, using the QUARC real-time control software (Quanser Consulting Inc., Markham, Canada).

A game was designed for the child to move the slave robot through a teleoperation system, in order to pick a token from box A in a 2D play environment and put it in box B (see Fig.3.6). A coil was mounted on the slave end-effector and charged with electrical current when the robot reached the box A for picking the metal token. This coil was discharged when the slave end-effector reached the box B for placing the token in this box. In this experiment, the child was simulated as a spring array which was pulled to the box A location at the beginning of the experiment (Fig.3.6(c)). One of the common symptoms

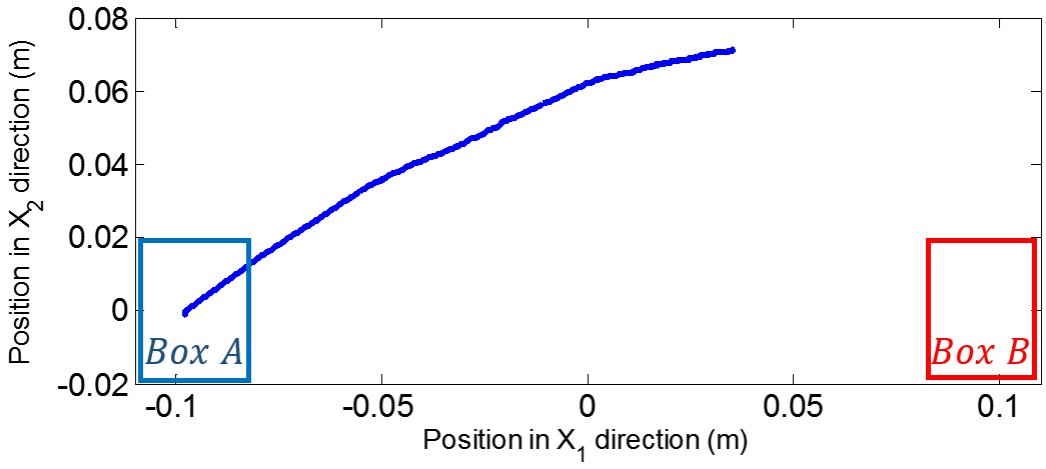

Figure 3.7: The simulated CP child (spring array) trajectory without therapist/robotic assistance.

of children with CP is their poor coordination and motor function [2]. So, it was expected that after releasing the spring array from Box A it produces 2D forces which are not toward the desired destination. Therefore, the spring array reached its equilibrium point, which was not the box B's location (Fig.3.7). Thus, the simulated child could not move the master, and consequently the slave, to the box B location and accomplish the pick and place task if unassisted. In [59] human hand dynamic is modeled as a spring array, which acts as muscle groups connected to joints. So, considering the muscle stiffness of children with CP [2], and passivity of interaction dynamics in robotic assistance, it is safe to simulate the movement of children with CP as a passive spring array. The same approach was considered in [10, 11] to simulate movements of people who had a stroke.

3.4.1 Demonstration Phase

The child (spring array in the reminder of this section) was unable to reach box B, therefore, it was required that in the demonstration phase that the therapist (author in the reminder of this section) assist the child to correct the movements by applying assistive/resistive forces to the slave end-effector

in the tangential/normal directions. The therapist intervention and assistance was minimal and on an as-needed basis. Also, the unique motion characteristic of the child was considered by the therapist to prevent any possible pain or discomfort. The motion characteristic was expected to be curve-like as observed in [18]. Accordingly, the therapist assisted the child through the teleoperation system to accomplish the task successfully. The obtained trajectories of the "child" and the therapist across 5 trials are shown in Fig. 3.8(a) The GMM of these trajectories are shown in Fig.3.8(b). The average demonstrated trajectory and the corresponding variation manifold obtained from GMR are also illustrated in Fig.3.8(c) . As seen in Fig.3.8, the GMM and GMR models efficiently captured the average and variability of cooperative task execution. The therapist interaction force in tangential and normal directions for the trial number 4 is sketched in Fig.3.9.

Based on the structure of the utilized spring array, the child was exerting a force in the normal direction along the trajectory. Thus, the therapist applied force in the opposite direction (Fig.3.9(b)) to increase resistance in normal direction and bend the mutual trajectory toward box B, while preserving the curve-like motion characteristic of child. In tangential direction, at first, the therapist applied force in negative direction to reduce the abrupt acceleration of the robots produced by the spring array at the Box A location (Fig.3.9(a)). Then, the therapist has provided the positive force to assist the child to reach the destination.

3.4.2 Robotic Assistance Phase

The demonstrated average trajectory of the child-therapist cooperation in the previous phase were employed in this phase to perform the task in the absence of the therapist. The child deviation (in this phase) with respect to the demonstrated average trajectory (from the previous phase) was determined as a response to his/her interaction forces, using the proposed tangential-normal

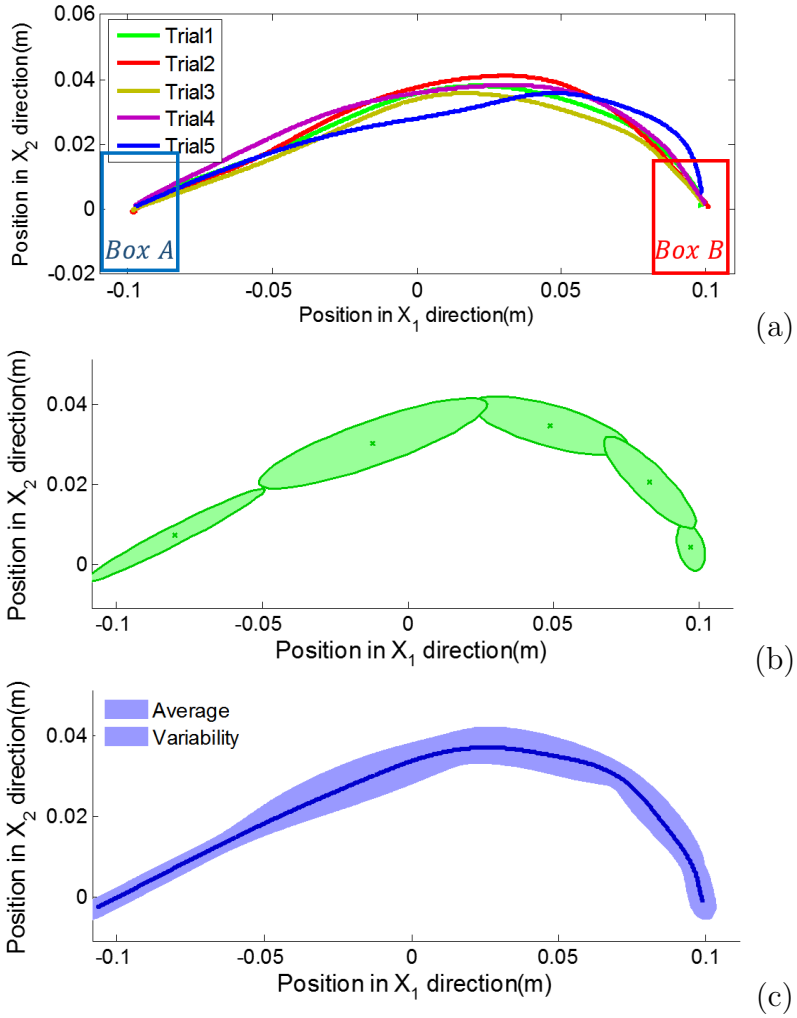

Figure 3.8: The cooperative task demonstration: (a) Therapist-child mutual position, executing the pick and place task for 5 trials, (b) the projection of 3D GMM on the $X_1 - X_2$ Cartesian coordinates, (c) the average and variability of the demonstrated trajectories, resulting from GMR.

impedance models (3.23), (3.24). In order to evaluate the performance of the impedance model in terms of adjustment of the child's freedom to deviate, different sets of impedance models were defined that are listed in Table. 3.1. Impedance parameters were chosen to provide the robot with appropriate transient response to child's input forces and cancel the high frequency response, which corresponds to tremor in children with CP:

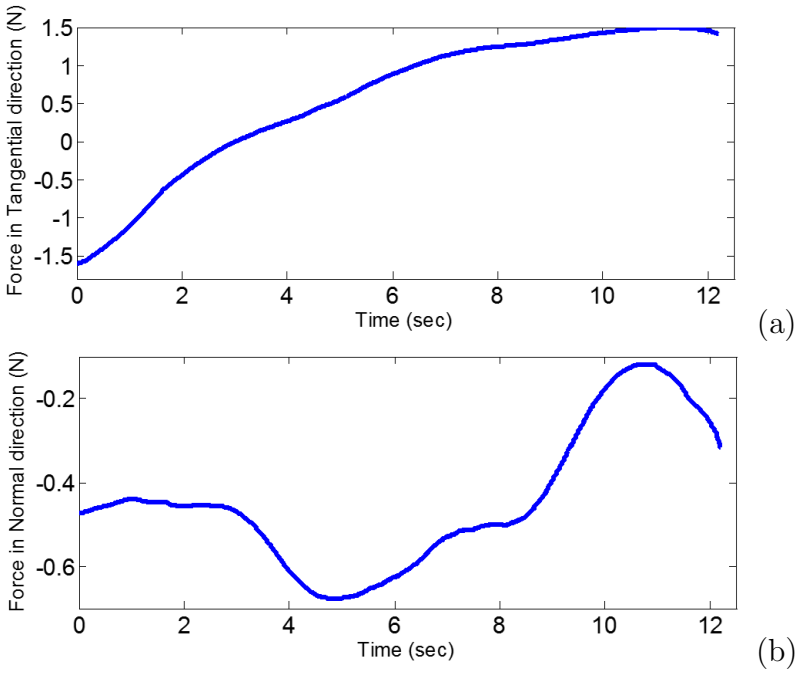

Figure 3.9: Therapist-applied force in the task demonstration: (a) in tangential direction, and (b) in normal direction.

$$\xi = c/2\sqrt{m.k} = 0.7 \tag{3.31}$$

$$\omega_n = \sqrt{m.k} = 2 \tag{3.32}$$

Using these parameters in the virtual impedance models and applying the proposed impedance control strategy to follow the average demonstrated trajectory, the $X_1 - X_2$ trajectory of the slave robot (in the task environment) was shown in Fig.3.10.

Impedance parameters adjust the trade-off between accuracy (more assistance/resistance) and flexibility (less assistance/resistance) in each of tangential/normal directions. Movement in the tangential direction highly contributes to the task accomplishment as the child is moving along the average demonstrated trajectory to reach the destination (box B). So, it is desirable to provide the child with more flexibility (less assistance) in the tangential direction to

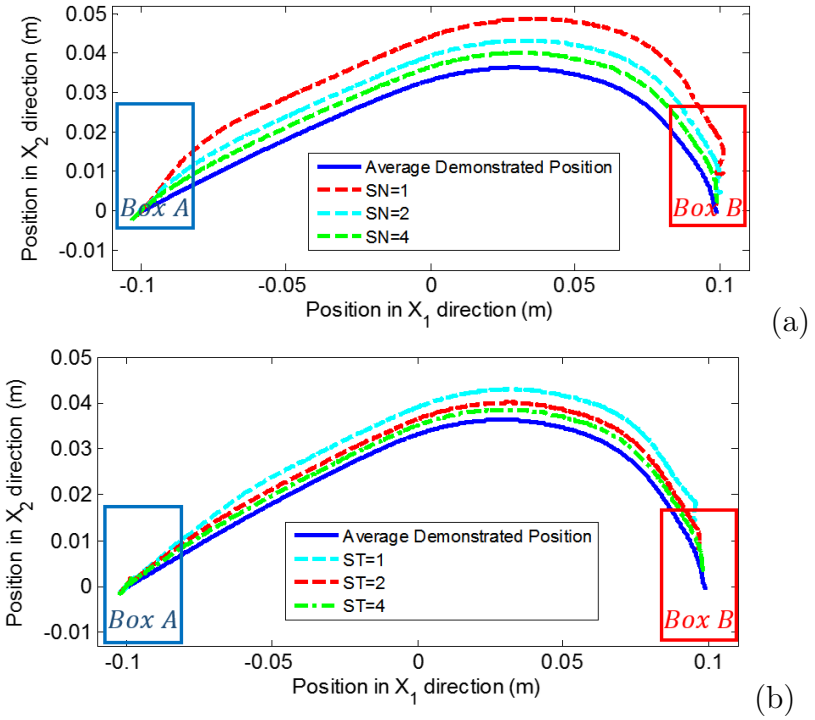

Figure 3.10: Robotic assistance phase. Child's trajectory: (a) more flexibility (less resistance) in the normal direction, and (b) more flexibility (less assistance) in the tangential direction.

$T < N$	M	C	K	ST
Tangential (T)	$50 \times ST$	$140 \times ST$	$200 \times ST$	$\{1, 2, 4\}$
Normal (N)	$100 \times ST$	$280 \times ST$	$400 \times ST$	
$N < T$	M	C	K	SN
Tangential (T)	$100 \times SN$	$280 \times SN$	$400 \times SN$	$\{1, 2, 4\}$
Normal (N)	$50 \times SN$	$140 \times SN$	$200 \times SN$	

Table 3.1: Adjustment of tangential and normal impedance models for various set of parameters.

ensure his/her motivation and participation in task execution. However, the child's ability to move along the average trajectory should be taken into consideration. As it is observed in Fig. 3.10, choosing the impedance parameters by adjusting $ST = 1$, the child is unable to reach the destination, because of inadequate assistance in the tangential direction.

Less resistance in the normal direction gives more freedom to the child

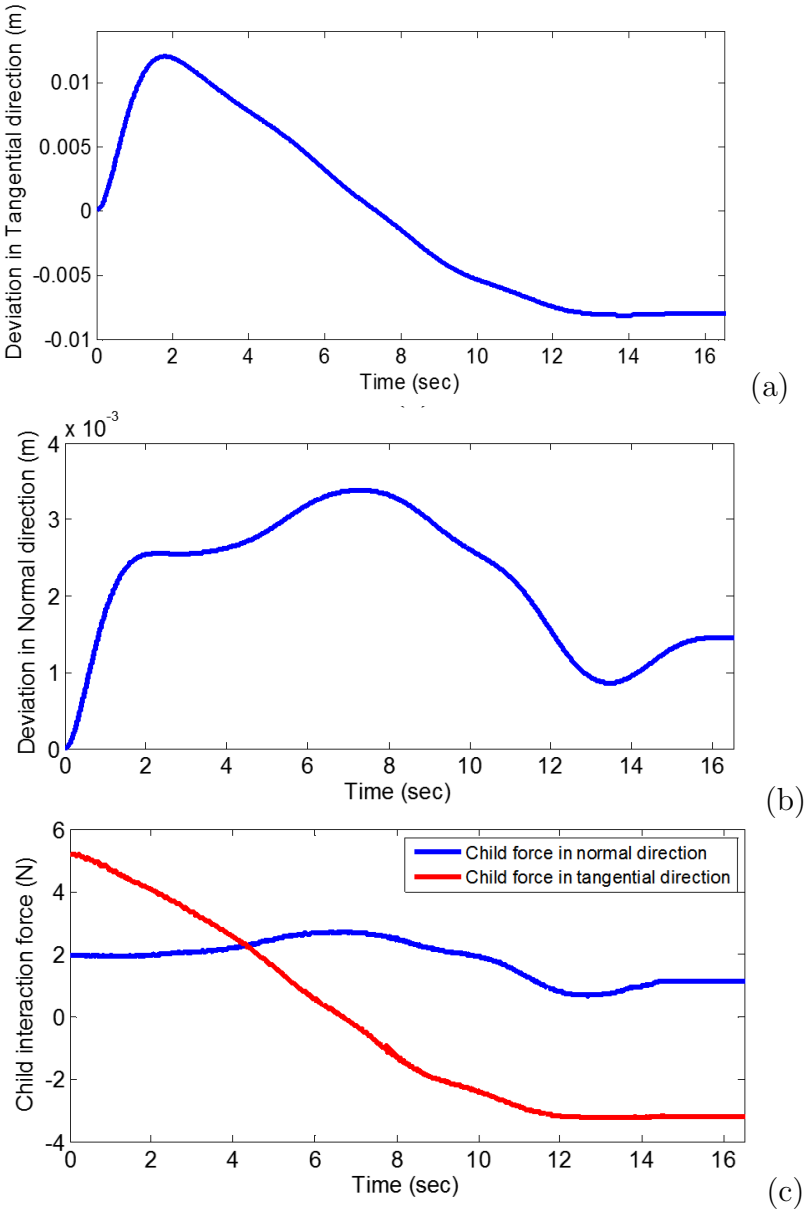

Figure 3.11: Robotic assistance phase ($ST = 2$): Child (a) deviation tangent to trajectory (b) deviation normal to the trajectory (c) interaction force in $T - N$ coordinates.

for deviation in directions orthogonal to the tangential direction. The level of flexibility in the normal direction is limited by any spatial restriction in the task environment. In order to minimize this resistance and also, meet the required accuracy for task accomplishment, this parameter can be set according to the observed variability of demonstrated data in Fig. 3.8(c).

Based on the above discussion, in this work, $ST = 2$ has been selected for the assistance phase, which the adjusted impedance parameters not only provided more flexibility in the tangential direction, but also allowsd the child to have acceptable deviation in normal direction. The corresponding position deviations from the average trajectory in the $T - N$ coordinates and also the applied interaction forces by the child in the $T - N$ directions that generate these deviations, are sketched in Fig.3.11.

3.4.3 Discussion

The proposed framework in this chapter has been experimentally validated by simulating the child interaction dynamic with a master robot as a spring array. As mentioned in Chapter 2, several assist as needed frameworks based on impedance/admittance controller have been suggested and even evaluated on actual patients [25] [20]. In this chapter, we extended this strategy by proposing a framework that utilizes LfD together with $T-N$ impedance controller, to learn the assistance needed and eliminate the need for robot programming and further intervention by the therapist. The proposed framework is applicable to provide assistance to children with CP, but clinical evaluation is out of the scope of this work. Moreover, using a spring array helped to better evaluate the proposed $T - N$ impedance controller, as it provides the same behavior in each reproduction trial. Point to point motion has been prevalently considered in both LfD and AAN literature for development and evaluation of frameworks, as it is the building block for motions with higher complexity [20, 60]. Thus, in this chapter, a simple pick and place task was considered to motivate the development of the robotic AAN framework. The proposed framework is able to produce complex movement trajectories as time index of position data is also captured in GMM and used as an independent variable to reproduce the movement via GMR. Also, the $T - N$ impedance controller imposes a virtual mass-spring-damper that models the dynamics between child and master robot

moving along the average trajectory produced by GMR. So, the robotic manipulator will follow the learned trajectory with adjustable flexibility for the child to deviate in each of tangential or normal directions.

3.5 Conclusion

In this chapter, a robotic-assistance-as-needed framework was proposed for children with Cerebral Palsy (CP) to perform a 2D position following task, by telemanipulating the slave robot in the play environment. In the first step (demonstration phase), the therapist interacted with the slave robot to assist and correct the simulated child's movements. A spring array was utilized to simulate the CP symptoms on the master robot. Using a learning from demonstration strategy, the Gaussian Mixture Model (GMM) and Gaussian Mixture Regression (GMR) techniques were utilized to approximate the average and variability of the demonstrated therapist-child trajectories. Then, in the robotic assistance phase (without therapist intervention), the impedance control method was applied such that the master robot provides a desirable flexibility for the child while following the average trajectory. Different impedance characteristics were defined for the child deviation in normal and tangential directions with respect to the average trajectory. As small as needed impedance parameters were employed in the tangential direction to provide appropriate flexibility (assistance) for the child to execute the task. However, by increasing the impedance parameters corresponding to the normal direction, the child deviation from the desired trajectory decreases. The validity of the proposed framework was experimentally evaluated by using different sets of impedance parameters in tangential/normal impedance models. In future works, the proposed strategy will be utilized with real children with CP to improve their ability and success rate in pick and place tasks in the play environment.

Chapter 4

Time-indexed Motion Learning with Tangential-Normal Varying Impedance Controller (TNVIC)

In this chapter, the therapist and the patient cooperatively perform a given task on a single robotic manipulator a few times. The therapist provides assistance such that the patient can complete the task, considering that more variability will result in less assistance to the patient (i.e., more freedom for the patient to deviate from the desired trajectory) in the reproduction phase. Then, using the GMM, the joint time-position data of demonstrated trajectories is captured statistically. Finally, in the therapist's absence, the GMR will extract the demonstrated average trajectory and also its trial-to-trial variability at each time from the GMM, same as in chapter. 3. However the proposed TNVIC in this chapter assists the patient to follow the average trajectory while imitating the therapist time-varying assistance based on the acquired variability (via impedance control) in tangential and normal directions (Fig.4.1). Other features and novelties of this chapter are:

- Unlike the previous RLfD frameworks for AAN [10, 11], where a varying PID controller was used to represent the variability observed in the

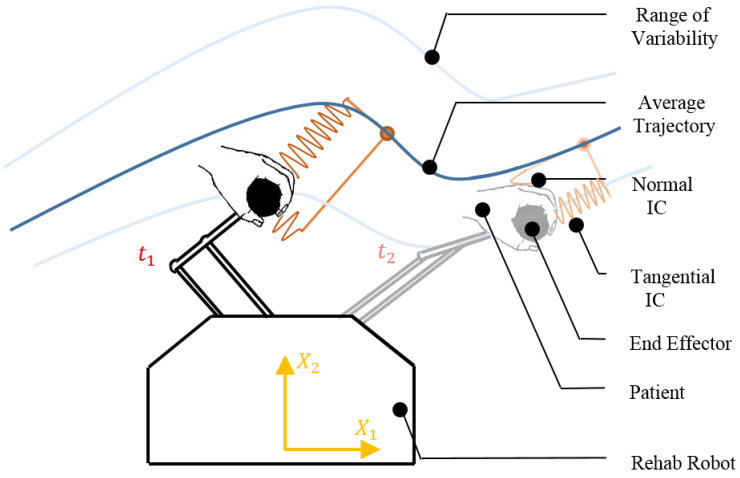

Figure 4.1: In the demonstration phase, the therapist and the patient cooperatively perform the task for a number of trials. Then, using robot learning from demonstration, the task is modelled as an average trajectory (centroid of virtual tunnel) and variations in trajectory (width of the virtual tunnel). The proposed TNVIC assists the patient by two varying impedance models (spring-damper) to follow the demonstrated trajectory and remain in the demonstrated range of variability. This figure shows the TNVIC in two time instances (t_1,t_2). The less the variability, the higher (the more stiff) the impedance models in tangential and normal directions to allow lower deviations by the patient about the average trajectory.

demonstrations of the task, in the proposed TNVIC we use impedance controllers that have been widely utilized in human-robot interaction to regulate the interaction between the patient and the robotic manipulator.

- In TNVIC, the impedance models vary inversely proportional to the demonstrated trial-to-trial variability with consideration of the maximum interaction force (by the patient) to accurately assist the patient to remain in the demonstrated range of variability. However in [55, 61], linear and sigmoid functions were used to approximate the inverse relation of impedance parameters and variability.

4.1 Cooperative Task Demonstration

Reaching motions are routinely part of rehabilitation exercises. For simplicity, the task is constrained to a 2-dimensional Cartesian space. It is assumed that the patient is unable to complete a given task, if unassisted. Therefore, the therapist also interacts with the robotic manipulator held by the patient in order to assist the patient to carry out the task, considering the patients constraints and range of motion. A few cooperative task trials are sufficient to demonstrate to the robotic manipulator the required assistance.

4.1.1 Data Sampling and Arrangement

During the demonstration phase, the 2-dimensional position signal in the Cartesian coordinates $\xi_p \in R^2$ and the time variable $\xi_t \in R$ are sampled and jointly denoted as ξ. Having M task demonstrations (i.e., trials), respectively consisting of $\{N^j, j = 1, \cdots, M\}$ samples, the entire demonstrated data can be organized as

$$D = \left\{ \{\xi^{i,j}\}_{i=1}^{N^j} \right\}_{j=1}^{M}, \forall \xi^{i,j} = \begin{bmatrix} \xi_p^{i,j} \\ \xi_t^{i,j} \end{bmatrix} \in R^3 \tag{4.1}$$

where $\xi^{i,j}$ represents the i^{th} sample of the j^{th} demonstration. The data (D) consists of $\sum_{j=1}^{M} N^j$ discrete samples.

4.1.2 Gaussian Mixture Model (GMM)

The GMM statistically models the demonstrated data by a sum of weighted Gaussians [60]. A Gaussian probability density function (PDF), also known as the normal distribution, has been widely used to model physical phenomenon such as human movements. A single Gaussian PDF is unable to capture inevitable nonlinearities in the complex trajectory-following tasks. Hence, the GMM uses a mixture of K individual Gaussians as shown in Fig.4.2 The GMM

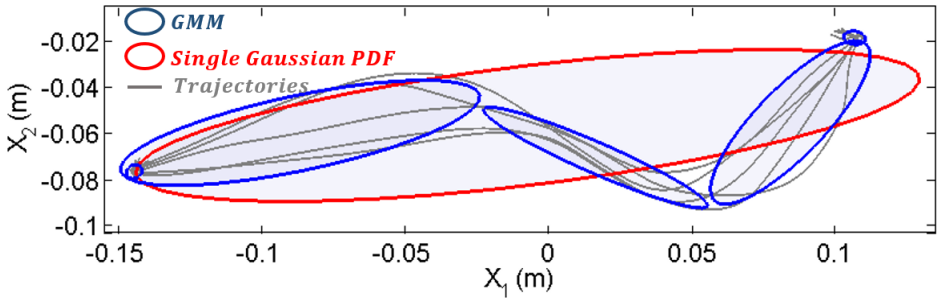

Figure 4.2: An example scenario where a GMM with its 5 clusters (Blue ellipsoids) captures the nonlinearities in demonstrated trajectories, as compared to a Single Gaussian PDF (Red ellipsoid). Note that this figure displays the reflection of the 3-dimensional trajectories and GMM over the 2-dimensional spatial axes.

as a PDF operator (f) that models the demonstrated data (D) with its variable is expressed as

$$f(\xi;\theta^i) = \sum_{i=1}^{K} \pi^i \mathcal{N}_3(\xi;\mu^i,\Sigma^i) \tag{4.2}$$

$$0 \ < \pi^i < 1 \ \ \& \ \sum_{i=1}^{K} \pi^i = 1 \ \ \& \ \Sigma^i = \begin{bmatrix} \Sigma_P^i & \Sigma_{P,t}^i \\ \Sigma_{t,P}^i & \Sigma_t^i \end{bmatrix} > 0 \tag{4.3}$$

where $\theta^i = \{\pi^i \in R^3, \mu^i \in R^3, \Sigma^i \in R^{3\times 3}\}$ are made up of parameters of the GMM, i.e., the prior weight, the mean and the covariance matrix for each of the K Gaussian components, respectively. $\mathcal{N}_n$ denotes the n-dimensional Normal PDF (Appendix I). The optimum number of components (K) is chosen, using Bayesian Information Criterion, which penalize the complexity of the GMM model [62]. The GMM parameters ($\{\theta^i\}_{i=1}^K$) are learned, using Expectation Maximization algorithm [42].

Now, all the discrete $\sum_{j=1}^{M} N^j$ samples, each consisting of a position variable ($\xi_p \in R^2$) and a time variable ($\xi_t \in R$), are modeled by the sum of K weighted Gaussian PDFs which capture the demonstrated trajectories in terms of its average and its variations in the position-time space.

4.2 Robotic Semi-Autonomous Assistance

In this section, the aim is to provide a framework to robotically reproduce the assistance provided by the therapist in order to assist the patient in completing the task in the therapists absence. For this purpose, at each time, the expected position captured by GMM is extracted via GMR. Then, using the proposed TNVIC, the user is assisted to reach this expected (desired) position, mimicking the therapist intervention by considering the demonstrated trial-to-trial variability in tangential and normal directions.

4.2.1 Gaussian Mixture Regression (GMR)

Extracting data from the learned 3-dimensional GMM in Section.4.1.2, and feeding it to the robot controller in real-time requires a regression technique to approximate the expected (desired) 2-dimensional position ξ_p in a given time $\xi_t = t$. In this work, GMR is used as a probabilistic operator that approximates a single Gaussian PDF of the expected position (ξ_p) by calculating a conditional probability on the learned GMM [9], as (3), in which $\widehat{\mu_{p,t}} \in R^2$ and $\widehat{\Sigma_{p,t}} \in R^{2\times 2}$ approximate the average and covariance matrices of the demonstrated position at a given time $\xi_t = t$. (Fig.4.3).

$$f(\xi_P|\xi_t = t; \theta^i) \approx \mathcal{N}_2(\xi_P; \widehat{\mu_{P,t}}, \widehat{\Sigma_{P,t}}) \tag{4.4}$$

4.2.2 Tangential-Normal Varying Impedance Controller (TNVIC)

The TNVIC assists the patient to follow the average demonstrated trajectory $\widehat{\mu_{p,t}}$ using two time-varying virtual spring-damper impedance models. In real-time, $\widehat{\mu_{p,t}}$ acts as a target moving along the average demonstrated trajectory. The impedance models (spring-damper) virtually connect the robot

end-effector (held by the patient) to the moving target ($\widehat{\mu_{p,t}}$), respectively in tangential and normal coordinate system $T-N$, as

$$c_{T,t}\dot{\widetilde{\xi}}_{P_T} + k_{T,t}\widetilde{\xi}_{P_T} = -F_{P_T} \tag{4.5}$$

$$c_{N,t}\dot{\widetilde{\xi}}_{P_N} + k_{N,t}\widetilde{\xi}_{P_N} = -F_{P_N} \tag{4.6}$$

where $\{c_{T,t}, k_{T,t}\} \in R^+$ and $\{c_{N,t}, k_{N,t}\} \in R^+$ denote the desired time-varying damping and stiffness in $T-N$. $\widetilde{\xi}_{P_T}$ and $\widetilde{\xi}_{P_N}$ indicate the deviation with respect to $\widehat{\mu_{p,t}}$, resulting from the patients force exertions in tangential (F_{P_T}) and normal (F_{P_N}) directions. The direction and magnitude of the two orthogonal impedance models vary based on the demonstrated average ($\widehat{\mu_{P,t}}$) and variability ($\widehat{\Sigma_{P,t}}$) as follows.

Direction: The impedance controllers rotate to be tangent/normal to the average demonstrated trajectory. The $T-N$ at a given time (t) is centered on the desired trajectory ($\widehat{\mu_{P,t}}$) and rotated with respect to an inertial Cartesian coordinate system $X_1 - X_2$ with angle

$$\theta_{R,t} = Arctan\Big(\Big(\widehat{\mu_{P_{X_2},t}} - \widehat{\mu_{P_{X_2},t-T}}\Big)\Big/\Big(\widehat{\mu_{P_{X_1},t}} - \widehat{\mu_{P_{X_1},t-T}}\Big)\Big) \tag{4.7}$$

where $\widehat{\mu_{P_{X_2},t}}$ and $\widehat{\mu_{P_{X_1},t}}$ represent the projection of $\widehat{\mu_{P,t}}$ on $X_1 - X_2$. T denotes the sampling period. Therefore the rotation matrix from $X_1 - X_2$ to $T-N$ would be

$$R_{R,t} = \begin{bmatrix} cos(\theta_{R,t}) & sin(\theta_{R,t}) \\ -sin(\theta_{R,t}) & cos(\theta_{R,t}) \end{bmatrix} \tag{4.8}$$

Magnitude: The impedance parameters are in inverse proportion relation to the variability of the demonstrated trajectories. Following Hookes law, with a constant force exerted by the patient on a spring that connects the robotic manipulator to the desired trajectory, the resulted deviation is inversely proportional to the spring magnitude (stiffness) as $\widetilde{\xi}_{P_T} = F_a/k$. Therefore, to mimic the therapists assistance (i.e., the therapist variable interaction stiffness), the

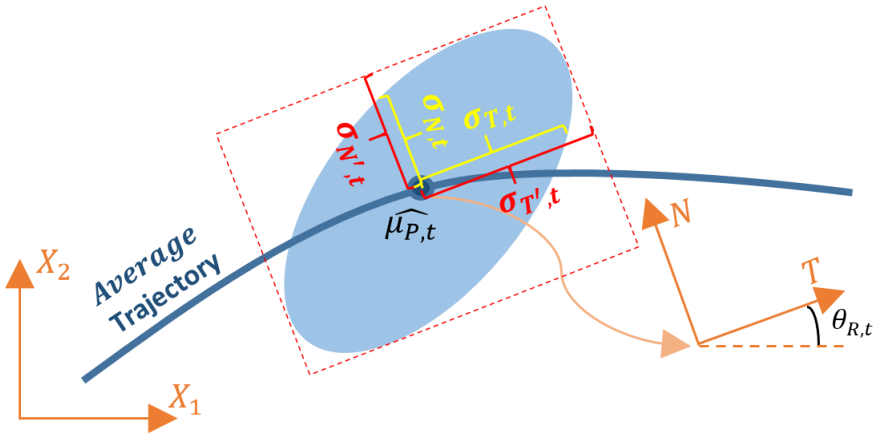

Figure 4.3: The calculation of standard deviation in tangential and normal directions, using (4.10) and (4.11).

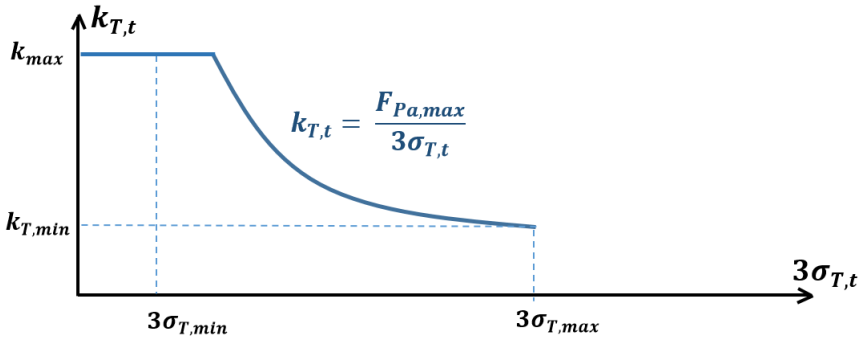

Figure 4.4: The inverse proportional relationship between stiffness and standard deviation in tangential direction when $k_{T,max}$ ($k_{T,t}$ when $\sigma_{T,t} = \sigma_{T,min}$) is larger than k_{max}.

spring magnitudes are selected inversely proportional to the demonstrated variability (as shown in Fig.4.4) in each of tangential and normal direction so that the patient do not deviate more than the demonstrated range of variability

$$\begin{aligned} &\{k_{\varsigma,t} = F_{P,max}/3\sigma_{\varsigma,t} \\ &if(k_{\varsigma,t} > k_{max}) \Rightarrow k_{\varsigma,t} = k_{max}\} \end{aligned} \tag{4.9}$$

where $\varsigma = \{T, N\}$, should be substituted with T or N syntaxes to represent the equation for variable spring value in tangential or normal directions, re-

spectively. k_{max} is the maximum stiffness determined by the user for hardware restriction. $\sigma_{\varsigma,t}$ denotes the demonstrated standard deviation along tangential ($\sigma_{T,t}$) or normal ($\sigma_{N,t}$) axis, which are extracted from rotated covariance matrix ($\widehat{\Sigma_{P_{T-N},t}}$)) at each time, calculated from (4.10) and (4.11). $3\sigma_{\varsigma,t}$ is the distance to the average in Gaussian PDF that contains %99 of demonstrated trajectories. $F_{P,max}$, is the patients maximum force, measured (or tuned) before robotic assistance.

$$\widehat{\Sigma_{P_{T-N},t}} = \begin{bmatrix} (\sigma_{T',t})^2 & \rho_t \sigma_{T',t} \sigma_{N',t} \\ \rho_t \sigma_{T',t} \sigma_{N',t} & (\sigma_{N',t})^2 \end{bmatrix} \tag{4.10}$$

$$\sigma_{\varsigma,t} = \sqrt{1-{\rho_t}^2}.\sigma_{\varsigma',t} \tag{4.11}$$

In (4.10) and (4.11), $\sigma_{N',t}$ and $\sigma_{T',t}$ represent the reflected standard deviation on $T-N$ axes as shown in Fig.4.3, ρ_t is the correlation factor, which is a constant value between zero and one.

To set the constant damping ratio (τ_ς) for the transient response of impedance models dynamics to the patients force input, the variable damper is calculated as

$$c_{\varsigma,t} = \tau_\varsigma k_{\varsigma,t},\ \varsigma = \{T, N\} \tag{4.12}$$

Finally, having the variable impedance models, and interaction force of patient (F_{Pa_T}) ,(F_{Pa_N}), the resulting deviation ($\widetilde{\xi}_{P_T}$), ($\widetilde{\xi}_{P_N}$), can be calculated from (4.5) and (4.6). The desired position ($\xi_{P,des}$) of the robotic manipulator followed by the PID position controller is the sum of the average demonstrated trajectory and patient deviation which are rotated back from $T-N$ to X_1-X_2 as:

$$\begin{bmatrix} \xi_{P_{X_1},des} \\ \xi_{P_{X_2},des} \end{bmatrix} = \begin{bmatrix} \widehat{\mu_{P_{X_1},t}} \\ \widehat{\mu_{P_{X_2},t}} \end{bmatrix} + (R_{R,t})^{-1} \begin{bmatrix} \widetilde{\xi}_{P_T} \\ \widetilde{\xi}_{P_N} \end{bmatrix} \tag{4.13}$$

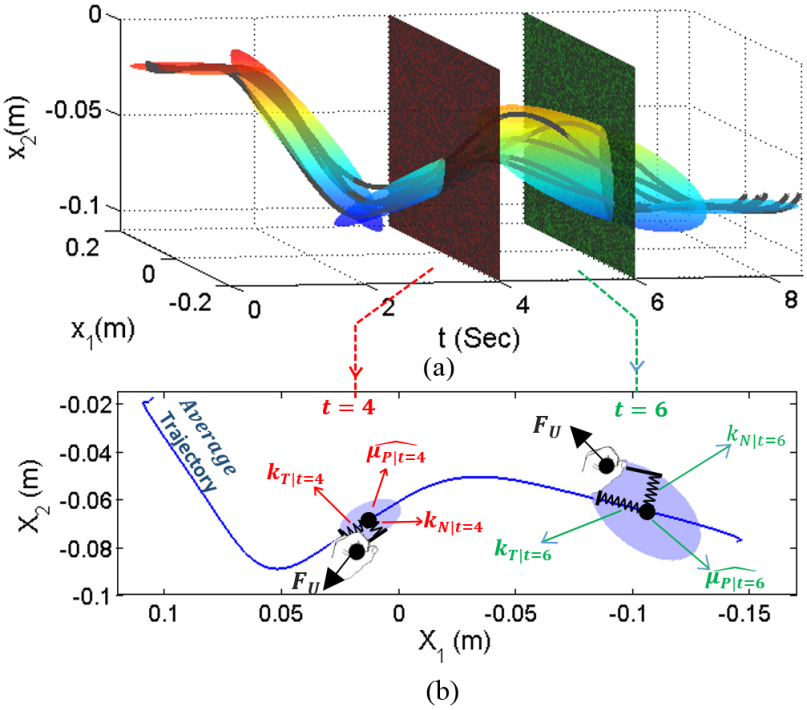

Figure 4.5: (a) The demonstrated trajectories (black lines) are modeled by a 3-dimensional GMM (ellipsoids) in joint position-time space (Section. 4.1.2). The planes normal to the time axis (t), represent the Gaussian Mixture Regression. The expected demonstrated position in a given time is calculated by approximating a single 2-dimensional Gaussian PDF from the intersected mixture models (Section .4.2.1). The times $t = 4$ and $t = 6$ are selected randomly to provide an example of the proposed robotic assist-as-needed framework. (b) Shows the proposed controller in ($t = 4$, $t = 6$).

The proposed TNVIC is shown in Fig. 4.5.

4.3 Experimental Validation and Discussion

The proposed framework is experimentally evaluated using a Quanser rehabilitation robot and implemented in QUARC real-time software (Quanser Consulting Inc., Markham, Canada) with a sampling frequency of 1 kHz. Without loss of generality, an application for assisting children with CP has been considered in this work. Playing is vital for childrens physical and mental cognitive development [63]. Nowadays, one of the common activities of children is using

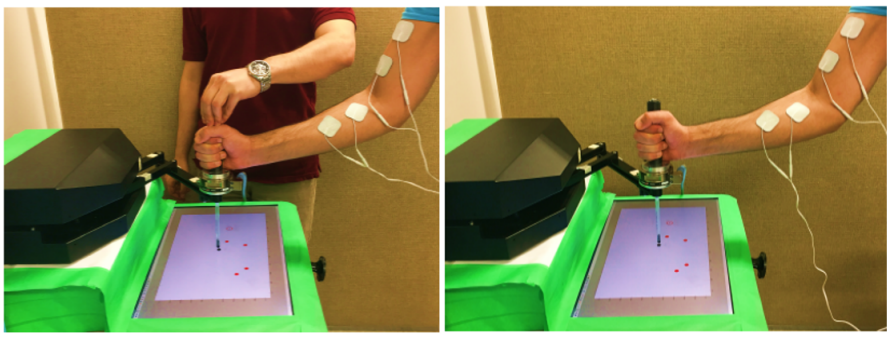

Figure 4.6: This figure shows the experiment setup in both demonstration (Left) and robotic assistance (right) phases. Two pairs of transcutaneous electrical nerve stimulation pads were used for simulation of CP symptoms (Section.4.3).

apps on smartphones, tablets, and touchscreens.In order to help children with CP to also have the same experience, the proposed framework can be used to assist them in tasks, which can be represented by point-to-point motion primitives. A designed 2-dimensional virtual game was projected on an LCD screen placed under the robotic end effector as shown in Fig.4.6. The user is expected to move the robotic end-effector (in contact with the LCD) from point A to point B, through two gaps with different directions and widths, as Fig.4.7.(a).

$\tau_\varsigma = 0.15sec$	$F_{P,max}$	$K_{max} = 1800\ N/m$

Table 4.1: The selected system parameters

4.3.1 Simulation of Cerebral Palsy (CP) Symptoms in An Adult Without Disability

The main symptoms of CP as discussed in Section. 2.1.1 are stiffness of muscles, limited range of motion, poor coordination, difficulties in performing a voluntary movement, weakness and tremor. In this experiment, to induce some of these symptoms the author (called patient later on in this section) was stimulated with transcutaneous electrical nerve stimulation (TENS) and performed

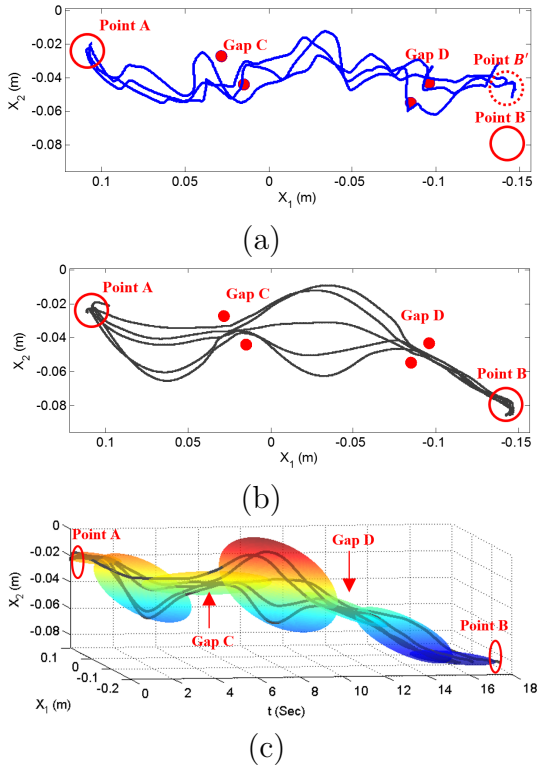

Figure 4.7: (a) The patient trajectories in 3 consecutive trials. Point $B^{'}$ is projecteod n the LCD monitor instead of the actual destination (point B) to simulate poor coordination in patients with CP (b) The cooperative demonstration of therapist and patient for 5 trials. The therapist intentionally demonstrated more variability in sections where less assistance (accuracy) were required. Also, as the patient has difficulty to coordinate his movements from gap D to point B, the therapist provided less variability in this section. (c) This graphic displays the 3-dimensional GMM with its seven Gaussian mixtures (colored ellipsoids) that modeled the position-time joint trajectories of the therapist demonstration (black lines) with its average and variability.

the experiments. Low-frequency stimulation of upper arm muscles (biceps) and wrist muscles (Flexor carpi, Palmaris lunges, etc.), was chosen to provide the maximum correlation with the behavior observed in an actual CP patient [42]. Also, in order to make the situation more challenging for the system, point $B^{'}$ was projected on the LCD instead of the actual destination (point$B$) to represent inability to accurately reach the destination. The adult user, in the presence of stimulation (called patient), was asked to perform the designed task and move from point$A$ to point$B$, while passing through Gaps C and D

without hitting them. As it is shown in Fig.4.7(a), the user was unable to correctly accomplish this task independently.

4.3.2 Demonstration

During the demonstration, a research assistant (called therapist for the reminder of this section) intervened in the task and provided the minimum required assistance. Considering the inverse correlation of the TNVIC assistance with the variability in the demonstrated trajectories, the therapist intentionally produced more variability between trials in regions where less assistance was required and vice versa (Fig.4.8(b)). The cooperative task trajectories (5 trials) were then captured by GMM to statistically model the task with its features (average and variability) as shown in Fig.4.8(c).

4.3.3 Robotic Assistance

Using the proposed TNVIC, and system parameters in Table. 4.1, the robotic system imitates the therapists time-varying intervention in the demonstration phase and assists the patient to complete the task successfully (Fig.4.6). The desired position data calculated via GMR from GMM, and varying tangential and normal stiffness (spring parameter magnitude) are shown in Fig.4.8. In this figure, t_C and t_D are associated with time instances that the average trajectory is in Gap C and Gap D, respectively. The patient is connected to the average trajectory with two virtual impedance models that regulate the level of assistance (stiffness) in each of tangential and normal directions. In Gap C and Gap D, due to the required accuracy, the therapist demonstrated low variability across trials. Therefore, it is expected to have a high level of assistance accordingly. As observed in Fig.4.8(b), at t_C and t_D, the variability (standard deviation) in the tangential direction is lower from the adjacent time, therefore the variable tangential spring is stiffer to provide more assistance. This is due to

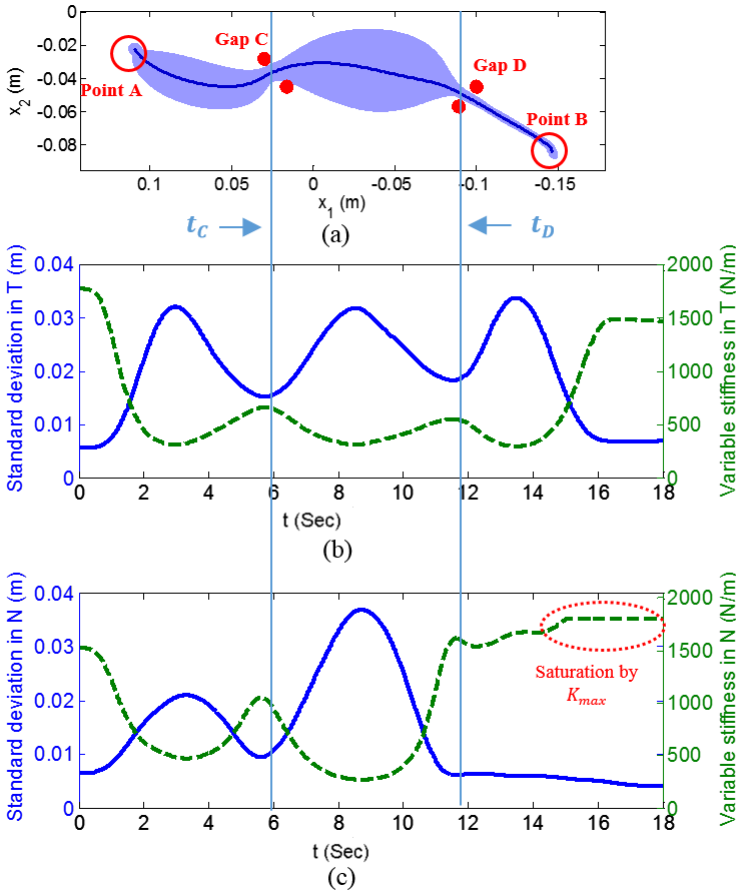

Figure 4.8: (a) This figure demonstrates the expected position probability density function (PDF) approximated by GMR from the GMM (Fig.4.7(c)) at all time samples in the robotic assistance. Note that in Fig.4.5(b), the GMR results have been shown just in two time instances. The dark blue dots and blue area display the average and variability for 2-dimensional Gaussians PDFs in all time samples, respectively. (b) At each time, the standard deviation in tangential (T) direction (Blue plot) is extracted from the 2 dimensional PDF approximated by GMR. The tangential variable spring value (Stiffness) changes with inverse correlation to the standard deviation (8) to assist the patient to remain in the demonstrated range of variability (3×standard deviation) in each time sample. (c) Same as (b), but in normal (N) direction.

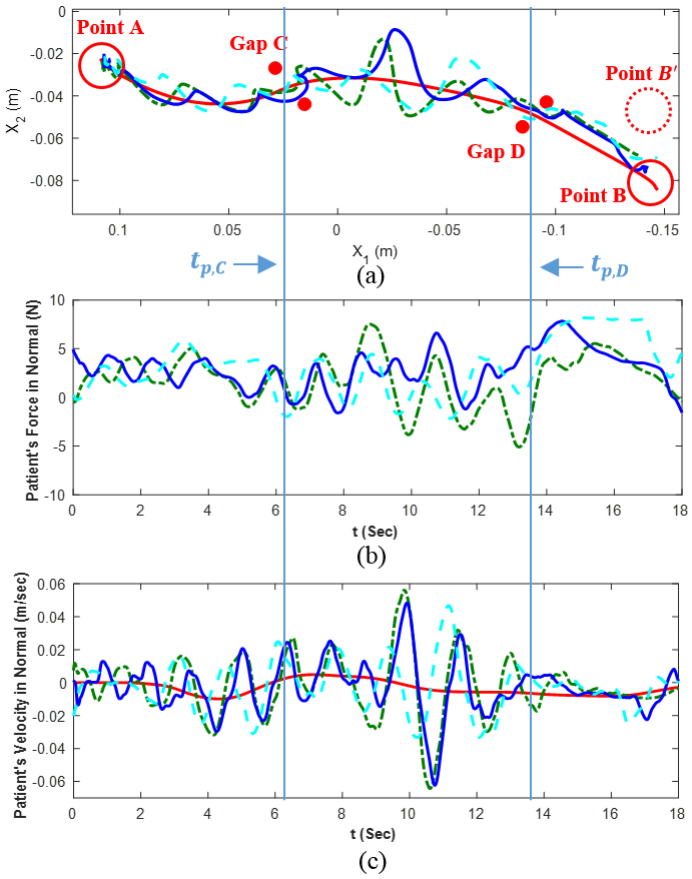

Figure 4.9: (a) Displays the patients trajectories in three consecutive task trials, being assisted by the robotic manipulator. The proposed TNVIC effectively assisted the patient to complete the task successfully.(The red plot is the average demonstrated trajectory) (b) Shows the patients interaction force with the robotic manipulator in normal direction. (c) Demonstrates the patient velocity in normal direction.

the fact that in demonstration, the therapist intuitively moved slower through sections where more accuracy was required. The same characteristic can be observed in the Normal direction as displayed in Fig.4.8(c). In gap C and gap D, the width of the path is narrower, thus more assistance is required in the normal direction, accordingly. As Gap D is narrower than gap C, the therapist demonstrated less variability in Gap D. Therefore the normal stiffness (assistance) is higher in t_D than in t_C. Using TNVIC, with its time-varying impedance models, the patient was assisted to perform the demonstrated task

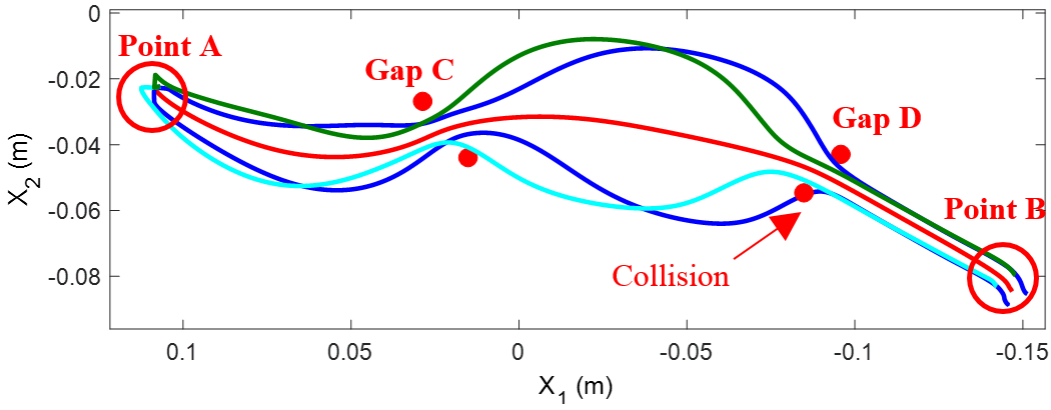

Figure 4.10: The performance of system when the users maximum force (10 N) is exerted on the system in 4 directions. $\{(F_{Pa_T}, F_{Pa_N})\}$ = (7.14, 7.14), (7.14, -7.14), (-7.14, 7.14), (-7.14, -7.14); all in Newton (N) . Note that as tangential normal directions are orthogonal, the projection of 10 N on each axis through Pythagorean law is 7.14 N

in contact with the robotic manipulator. Again, the point B', was projected on the LCD as the destination point, to test if the system can assist the patient to reach the actual destination (point B). Fig.4.9(a), displays that the patient successfully completed the task and moved from point A to point B, through gaps without hitting them. Fig.4.9(b), shows the interaction force of the patient in the normal direction. After Gap D, towards the destination (Point B), the patient exerted his maximum force to reach point B' (which he thinks is the destination). The controller successfully restricted the patient movement and dragged (assisted) his hand to the actual destination (point B). Between $t_{p,C}$ and $t_{p,D}$ (associated with approximate time instances that the patient passed through gap C and gap D, respectively), the stiffness parameters were lowest in both tangential and normal directions (Fig.4.8). Therefore, there was higher freedom for the patient to deviate. This extra freedom resulted in more intervention from the patient with the robotic manipulator as force exertion is increased. That is the cause for larger variations observed between $t_{p,C}$ and $t_{p,D}$, compared to $t < t_{p,C}$ in Fig.4.9. The advantage of the proposed framework is to provide maximum possible freedom to the patient (assist-as-needed)

to motivate him/her for participation in task execution.

In TNVIC, the variable impedance parameters were adjusted to restrict the patient from deviating out of the expected position along tangential and normal directions, even if he/she exerts his/her maximum interaction force. Therefore, any force exertion less than the measured (or tuned) maximum force, will end up in successful task completion, regardless of its direction and frequency. In Fig.4.10, the robotic system was introduced with the patients maximum force in 4 different directions (these values are assigned in the real-time controller) to observe the performance under some worst-case scenarios. As it is observed, just in one of the trials ($F_{Pa_T} = 7.14N, F_{Pa_N} = 7.14N$) there was a collision with Gap D. The possible sources of this error are: 1) The robot position controller (PID) as it has a transient response time to reach the desired position. 2) The sudden increase in impedance parameters, before entering the Gap D (Fig.4.8(c)). The impedance model is a dynamic system with tunable transient damping ratio (τ_ς), so it cannot keep up accurately with sudden changes in the desired trajectory. These constraints can be considered by possibly adding a penalty factor to (4.9).

In this experiments, a single trajectory-following task was successfully tested, however, the proposed framework is able to model complex trajectories as it uses GMM/GMR technique to model and reproduce tasks through time indexing. Also, sequential tasks can be learned and reproduced by several point-to-point motion primitives. Furthermore, using GMM/GMR, only a few demonstrations are required to capture the trajectory smoothly and effectively as opposed to simply averaging the demonstrated trajectories. Also, the GMM captures the variability of trials and statistical correlation of task variables which are utilized in this chapter to learn the therapist's intended interaction impedance. The interaction impedance is actively controlled in the robotic assistance phase, inversely proportional to the variability across trials in the demonstration phase to reproduce the intended time-varying impedance of the

therapist.

All in all, the proposed framework has merits in rehabilitation and assistive technologies to replicate the therapist's short intervention in trajectory-following tasks that have to be repeated several times. However the proposed system is task-specific and open-loop as the trajectory is generated by time rather than the current state of the system.

4.4 Conclusion

The framework, with its robot learning from demonstration (RLfD) framework and tangential-normal varying-impedance controller (TNVIC), were developed precisely in this chapter for an application in an assist-as-needed robotic system. The performance of the system in providing assistance with variable interaction dynamic (TNVIC) was evaluated in demonstration, RLfD, and semi-autonomous robotic assistance phases, with an adult induced with CP symptoms, using transcutaneous electrical nerve stimulation.

Chapter 5

Position-Indexed Motion Learning Using Potential Field Functions with Variable Dissipative Field

In the previous RLfD approach in chapter 3 and chapter 4 we used Gaussian Mixture Models (GMM) to mathematically capture the therapist-patient cooperative trajectory in the demonstration phase with its average (i.e., trajectory) and variability. Then Gaussian Mixture Regression (GMR) was performed in the robotic assistance phase, to reproduce the demonstrated trajectory in time. There are three ways to improve upon the previous approach. First, it should be noted that the assistance provided by RLfD algorithms in the traditional way is time-dependent [9]. This implies that the patient is required to follow the demonstrated trajectory at a similar velocity as in the demonstration phase. Otherwise, the robot increases the applied force to drag the user's hand on the desired path. Since the robot applies forces that are proportional to the deviation from the desired trajectory, the patient will experience a different level of assistance (i.e., higher or weaker forces) when interacting solely with the

robot as compared to with the therapist. The third way to improve upon past works naturally regards addressing safety issues that the first two points represent. In this chapter, we further extend the idea of RLfD for robotics-assisted rehabilitation to address these three points.

To simultaneously capture both the demonstrated trajectory and its impedance properties learned from therapist demonstrations, we propose a framework that uses a non-parametric potential field function introduced in [12]. Firstly, robot motion and impedance are captured by the non-parametric potential function's gradient and curvature, respectively, using a convex optimization algorithm. Then, in the therapist absence, the robot not only provides the patient with the same assistance he/she received during the task demonstration but also with a proposed performance-based and stable active variable the dissipative field that assists/resists the patient if he/she is following the trajectory slower/faster than the demonstrated velocity. Due to the application of the framework, there is an interaction between human and robotic manipulator. Patient's behavior can be non-consistent and variable, therefore the system requires to address the variabilities with the proposed velocity field controller. Usually, through the therapy sessions, the patient may get tired and requir excessive assistance, or they may exert extra force to the robotic manipulator because of the lack of coordination and muscle control. Also a perturbation in the task environment can alter the required assistive force for task accomplishment. To address this issue and increase the robustness of the model, the velocity field controller is proposed to regulate the patient's deviation from the velocity demonstrated by the therapist.

All in all, the potential field function acts as a valley around the trajectory that dictates the position-based force to the robot, and the velocity field controller can be represented by a river around the vicinity of the trajectory that introduces resistive/assistive force if the object (robot) is moving slower/-faster than the velocity of the river flow. The properties and advantages of the

proposed framework are:

1. Unlike chapter 3 and chapter 4 [8, 9], where only the *position* trajectories in the demonstrations were captured, in this chapter, by using potential function fields, the optimization goal and controller are modified and adapted to the context of robotic assistance to generate motions that also follow the same *force* profile experienced during the demonstration.

2. The proposed framework is capable of modeling and reproducing not only the position-following tasks as in chapter 3 and chapter 4, but also impedance-based tasks which represent most of our everyday activities (playing, opening a fridge door, cutting, etc).

3. Unlike Chapter 3 and chapter 4, the proposed controller has bounded force ranges that guarantees the stability and safety of the robot when in contact with passive environments.

4. As opposed to [12], an active time-variant velocity field controller is also augmented to regulate the level of patient's deviation from the velocity observed in the demonstration phase, using a tunable deviation tolerance variable that can be set based on the task and the patient's limitations.

The remainder of this chapter is organized as follows. Section. 5.1 introduces the cooperative task demonstration phase, subsequently used in Section. 5.2 in order to derive the modified potential field function. In Section. 5.3, we propose the velocity field controller and prove the stability of the overall system. Finally, in Section. 5.4, we validate the proposed approach in a 2-dimensional Cartesian space task using a planar rehabilitation robot.

5.1 Cooperative Task Demonstration

It is assumed that the patient is unable to complete a given task, if unassisted. Therefore, the therapist also interacts with the robotic manipulator held by

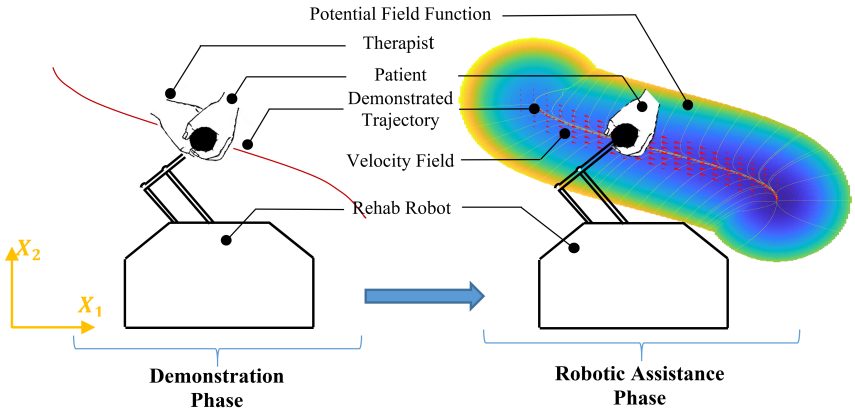

Figure 5.1: Displays the proposed framework for learning the therapist's assistance by demonstration. In the demonstration phase (Left), the therapist assists the patient to follow the trajectory for a single time. Then in robotic assistance phase (Right), by using potential field function and velocity field controller, the demonstrated therapist assistance is modeled and provided to the patient.

the patient in order to assist him/her to carry out the task, considering the patient's physical constraints and range of motion. The therapist provides the minimum-required assistance to motivate the patient to actively engage in the task. In this framework, just a single demonstration is required to learn the therapist's task-specific assistance.

The nonlinear dynamics of the multi-degrees of freedom (DOF) rigid robot in the n-dimensional Cartesian coordinates can then be given by

$$M(q_r)\ddot{x}_r + C(q_r, \dot{q}_r)\dot{x}_r + G(q_r) + f(\dot{x}_r) = F_{pa} + F_{ext} + F_c, \tag{5.1}$$

where $q_r \in R^{n\times 1}$ is the joint angles, $x_r \in R^{n\times 1}$ is the position of the robot end-effector in the Cartesian coordinates, $M(x_r) \in R^{n\times n}$ is the inertia matrix, $C(x_r, \dot{x_r}) \in R^{n\times n}$ contains Coriolis and centrifugal terms, $G(x_r) \in R^{n\times 1}$ contains position-dependent forces such as gravity, $f(\dot{x_r}) \in R^{n\times 1}$ is the friction force. Also, $\{ F_{pa}, F_{ext}$ and $F_c\} \in R^{n\times 1}$ are the patient, the external, and the control forces, exerted on the robotic end-effector, respectively. Note that as the robotic manipulator interacts with the task environment, the therapist

pulls/pushes the robot in order to assist the patient to completing the task.

When the robotic end-effector is in contact with both the patient and therapist, as they are cooperatively performing the task, let

$$\begin{aligned} F_{ext} &= F_{th} + F_{env} \\ F_c &= 0, \end{aligned} \tag{5.2}$$

in (5.1), where F_{th}, and $F_{env} \in R^{n\times 1}$ are the force applied by therapist and and task environment to the robotic manipulator, respectively.

5.1.1 Data Sampling and Preprocessing

During the demonstration phase, the n-dimensional position $x_P \in R^n$, velocity $\dot{x}_p \in R^n$ and interaction force between the therapist and the patient $F_{in} \in R^n$ in the Cartesian coordinates are sampled with a constant sampling time. Since the position vector samples are not evenly distributed along the trajectory, as velocity is not constant, the dataset is down-sampled to M evenly-distributed samples spatially to form the following dataset

$$D = \{[x_p^i; \dot{x}_p^i; F_{in}^i \in R^n] \in R^{3n}\}_{i=1}^{M} \in R^{3n\times M}, \tag{5.3}$$

where the superscript i is for the i^{th} sample of the demonstrated trajectory containing M samples in total.

Now, the tangential-normal coordinate system in the i^{th} sample ($\{T-N\}^i$) is defined, which is centered at x_p^i and with the tangential axis toward the next sample (x_p^{i+1}). The rotation matrix between the $\{T-N\}^i$ and inertial Cartesian coordinate system can be calculated via n rotation about inertial axes by Euler angles as

$$R_p^i(\theta_p^i) = R_p^i(\theta_{p_1}^i) R_p^i(\theta_{p_2}^i) \dots R_p^i(\theta_{p_n}^i) \tag{5.4}$$

Therefor, F^i_{in} and x^i_p can be represented in $\{T-N\}^i$, with the tangential $\{x^i_{p,T}, F^i_{in,T} \in R\}$ and normal $\{x^i_{p,N}, F^i_{in,N} \in R^{n-1}\}$ components, through the rotation matrix $R^i_p(\theta^i_p)$ as

$$\begin{aligned} [\dot{x}^i_{p,T}\ \dot{x}^i_{p,N}]^T &= R^i_p(\theta^i_p)\dot{x}^i_p \\ [F^i_{in,T}\ F^i_{in,N}]^T &= R^i_p(\theta^i_p)F^i_{in} \end{aligned} \quad \forall i \in \{1,2,...,M\}. \tag{5.5}$$

5.2 Learning Potential Field Function

This section introduces a framework to robotically reproduce the assistance the therapist provides in order to assist the patient in completing the task. For this purpose, potential function learning, which was firstly proposed in [12] is used. In the reproduction phase, the therapist is not present and the robotic manipulator provides assistance through the control signal F_C, such that in (5.1) we have

$$\begin{aligned} F_{ext} &= F_{en} \\ F_c &= F_{pot}(x_r) + F_{vel}(x_r, \dot{x}_r) \end{aligned} \tag{5.6}$$

in which

$$F_{pot}(x_r) = -\nabla U(x_r) \in R^n \tag{5.7}$$

is the gradient of the positive scalar potential field at each position ($U(x_r) \in R^+$). $F_{vel}(x_r, \dot{x}_r) \in R^n$ denotes the velocity field controller in the task environment.

In order to provide identical assistive forces as demonstrated to the patient to perform the point-to-point motion learning, two fundamental set of forces are required;

1. The attracting force $F^i_{in,N}$, which is normal to the trajectory and attracts

the end-effector and prevents the patient from deviating from that trajectory.

2. The propelling force $F^i_{in,T}$, which is tangent to the trajectory and assists the patient to go along the trajectory and reach the destination.

To jointly generate both of the tangential and normal forces, the non-parametric potential field is created by connecting the current position of the end-effector x_r to each sample x^i_p through a virtual spring model with stiffness K as

$$u^i(x_r) = u^i_0 + \frac{1}{2}(x_r - x^i_p)^T K^i (x_r - x^i_p) \ \forall i \in \{1, 2, ..., M\}. \tag{5.8}$$

Here $u^i_0 \in R^+$ is the bias potential and $K^i \in R^n$ is a diagonal stiffness matrix in the i^{th} position sample. The higher the stiffness matrix, the higher the attracting force $K^i(x_r - x^i_p)$ towards the i^{th} sampled position.

In order to smooth out the accumulated potential field produced by all of position samples, Gaussian kernel regression is used to produce the total potential energy as in[12] through the weighed average

$$U(x_r) = \sum_{i=1}^{M} \widetilde{\omega}^i(x_r) u^i(x_r) \tag{5.9}$$

with

$$\widetilde{\omega}^i(x_r) = \frac{\omega^i(x_r)}{\sum_{i=1}^{N} \omega^i(x_r)}, \tag{5.10}$$

and

$$\omega^i(x_r) = e^{-\frac{1}{2\sigma_i^2}(x_r - x^i_p)^T (x_r - x^i_p)} \tag{5.11}$$

where $\sigma^i > 0$ is a smooth parameter, $0 < \widetilde{\omega}^i(x_r) < 1$, and $\sum_{i=1}^{N} \widetilde{\omega}^i = 1$. As shown in Fig.5.2 , u^i_0 and K^i determine the tangential gradient and normal gradient of potential field, respectively. In the proposed robotic assistance scenario, the potential field parameters (u^i_0 and K^i) are set to represent the interaction performance of the therapist during the cooperative task demon-

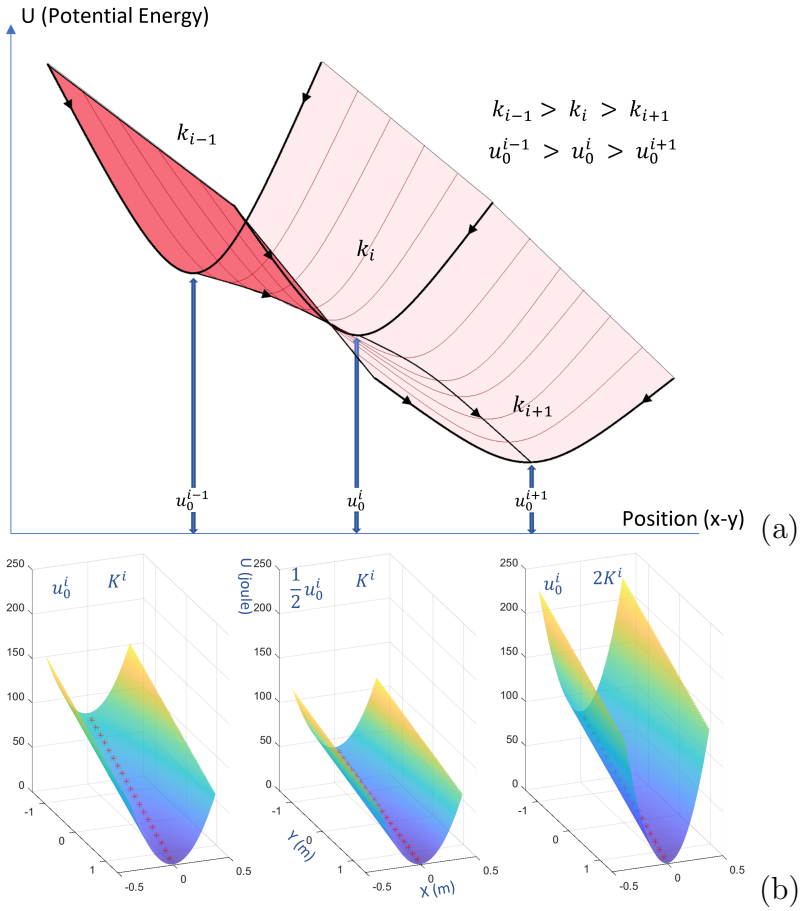

Figure 5.2: (a) Displays a small section of a potential field function that modeled a trajectory along three samples. The potential energy produced by stiffness parameters (K^i) increases proportionally to the distance from samples (5.8). Samples are close to each other, thus the stiffness parameter's effect on a potential gradient (i.e., force) in the tangential direction is negligible and it is approximately determined by the difference in bias potentials (u_0^i). (b) illustrate the effect of u_0^i and K^i parameters that alter the potential field gradient (i.e., force) in tangential and normal directions, respectively.

stration with the patient.

To replicate the therapist's normal force along the trajectory, the stiffness matrix is set to be diagonal and linearly proportional to the demonstrated normal interaction force as (5.12). Therefore, the robotic system will assist

(i.e., attract) the patient toward the trajectory where it is needed.

$$K^i = \begin{bmatrix} K_T^i & & & 0 \\ & K_{N_1}^i & & \\ & & \ddots & \\ 0 & & & K_{N_{n-1}}^i \end{bmatrix} \tag{5.12}$$

$$K_{N_j}^i = \frac{F_{in,N_j}^i - F_{in,N_j,min}}{F_{in,N_j,max} - F_{in,N_j,min}}(K_{N_j,max} - K_{N_j,min}) + K_{N_j,min}, \quad \forall j \in \{1, 2, ..., n-1\}. \tag{5.13}$$

where $F_{in,N_j,max}$ and $F_{in,N_j,min}$ are the maximum and minimum normal interaction force observed in j^{th} normal direction in the demonstration phase. Also, the $K_{N_j,max}$ and $K_{N_j,min}$ are the maximum and minimum stiffness parameters in j^{th} normal direction tuned based on the task-specific requirements and robot physical restrictions (e.g. actuator torque). In the next step, the u_0^i are leaned based on a convex optimization method so that the gradient of the potential field in tangential direction (i.e., $-\nabla u^i(x_p^i, \Theta)$) is equal to the assistive interaction force observed in the demonstration phase by the therapist to the patient in each sample (i.e., ${F_{in,T}^i}^+$). We use

$$\min \ J(\Theta) = \sum_{i=1}^{n} \|\nabla u^i(x_p^i, \Theta) + {F_{in,T}^i}^+\|_2, \tag{5.14}$$

subject to

$$\begin{aligned} & u_0^{i+1} \leq u_0^i, \quad \forall i \in \{1, 2, ..., T\}, \ i \neq \Omega, \ i+1 \neq \Omega, \\ & u_0^i \geq 0, \qquad \forall i \in \{1, 2, ..., T\}, \ i \in \Omega, \\ & \nabla \phi(x_p^*, \Theta) = 0, \end{aligned} \tag{5.15}$$

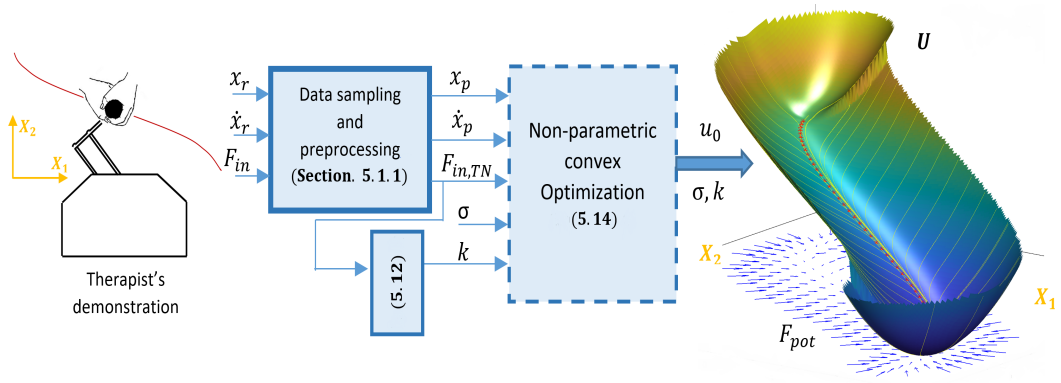

Figure 5.3: Illustrates the proposed Framework for Learning the therapist's assistive interaction force from the demonstration, using potential field function in Section. 5.2. x_r, $\dot{x}_r$ and F_{in} are recorded during the therapist's assistance demonstration to patient. And then down-sampled and processed (Section. 5.1.1) to be provided to the convex optimization which finds to optimum u_0 in the potential field to replicate the tangential interaction field provided by the therapist (5.14).

where Ω is a set of indices that correspond to the last point of each demonstrated trajectory, at the target point x_p^*, with $\Omega = \{i | x_p^i = x_p^*\}$. Also, in (5.14),

$$\nabla u^i(x_p^i, \Theta) = -\sum_{i=1}^{M} \frac{\widetilde{\omega}^i(x_r)}{(\sigma^i)^2}(u(x_p^i) - U(x_p^i)) + .. \\ \widetilde{\omega}^i(x_r)K^i(x_r - x_p^i) \quad (5.16)$$

and

$$F_{in,T}^{i\ +} = \begin{cases} F_{in,T} & \text{if } F_{in,T} >= 0 \\ 0 & \text{otherwise} \end{cases} \quad (5.17)$$

The convex optimization in (5.14) finds the optimized bias potential parameter (u_0^i) so the learned potential field dictates a position-related force equal to the therapist-demonstrated interaction force and exerts it on the patient's hand via the robotic end effector.

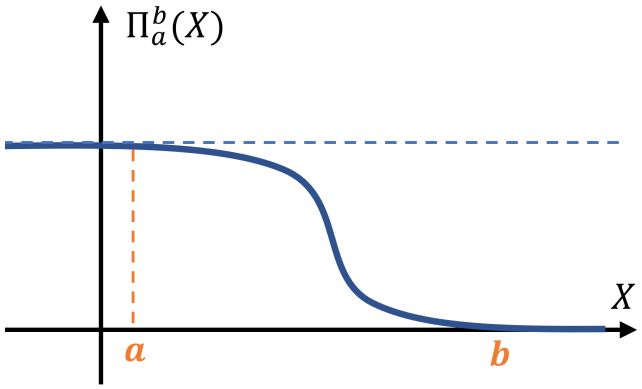

Figure 5.4: shows the smooth transition function used in (5.19) to smoothly decrease the desired velocity field as the distance from the trajectory increases

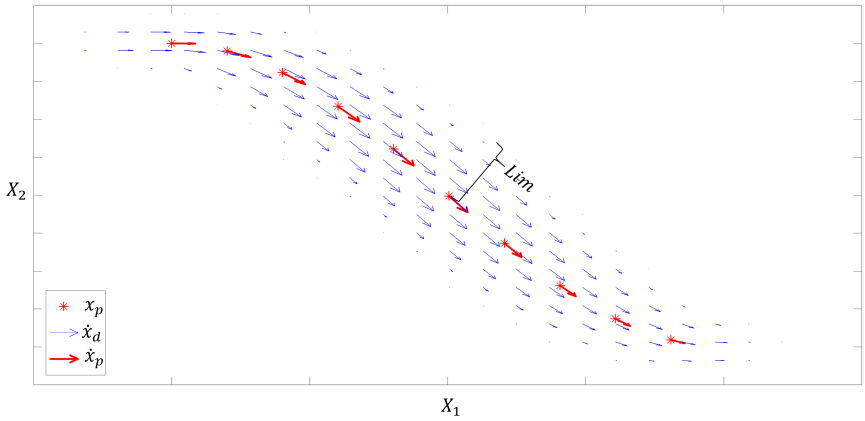

Figure 5.5: Illustrates the desired velocity field ($\dot{x}_d$) calculated by weighted average of the demonstrated velocities in data samples($\dot{x}_p^i$) as (5.18) in vicinity of the trajectory. *Lim* in (5.18) determines the maximum distance in which desired velocity field can exist

5.3 Velocity Field Controller

The learned non-parametric potential field in Section. 5.2 models the therapist-demonstrated interaction force but it has no control over the patient's velocity in the robotic assistance. Therefore, in this section, a velocity field controller is defined to adjust the transient response of the system and regulate the patient's velocity around the one demonstrated by the therapist. In the first step, the desired velocity in each position is calculated by the weighted average of the

demonstrated velocity as

$$\dot{x}_d(x_r) = \Pi_0^{Lim}(dis(x_r, x_p)) \sum_{i=1}^{M} \widetilde{\omega}^i(x_r)\dot{x}_p^i \tag{5.18}$$

where $\dot{x}_d(x_r) \in R^n$ represents the position-based desired velocity. $\dot{x}_p \in R^n$ denotes the demonstrated velocity in each sample. and $\Pi_0^{Dis} \in R^+$ is the smooth transition function (Fig.5.4) which can be chosen from the sigmoid function family as

$$\Pi_a^b(x) = \frac{1}{2} - \frac{1}{2}tanh(\frac{6(x - \frac{a+b}{2})}{b-a}) \tag{5.19}$$

In (18), $Lim \in R^+$ denotes the width of the velocity field, and $dis(x_r, x_p) \in R^+$ expresses the minimum distance of x_r from the position samples x_p. As demonstrated in Fig.5.4, the smooth transition function is added to limit the width of the velocity field to the trajectory. The aim is to minimize the interference of the velocity field with potential field and ensure the asymptotic stability of the accumulated field. In areas away from the trajectory, the potential field gradient (i.e., force) is mainly normal to the trajectory. This normal force pushes the patient towards the trajectory and helps with stability and accuracy of the patient in trajectory following tasks. Therefore, any added velocity field (which is aimed to be followed by the patient) will interfere with this normal force and threat the asymptotic stability toward the destination position. However, in the vicinity of the trajectory, the potential field gradient is mainly tangential, and the augmented velocity field would even help the asymptotic stability toward the destination. The potential and velocity fields are jointly sketched in Fig.5.5.

Now, in order to regulate the robot's velocity around the desired one, we use the varying dissipative field controller proposed in [46]. This controller separately regulates the velocity in the tangential direction and selectively dissipates energy in the direction normal to the desired velocity. This is achieved by a full ranked variable damping matrix, whose orthogonal eigenvectors ro-

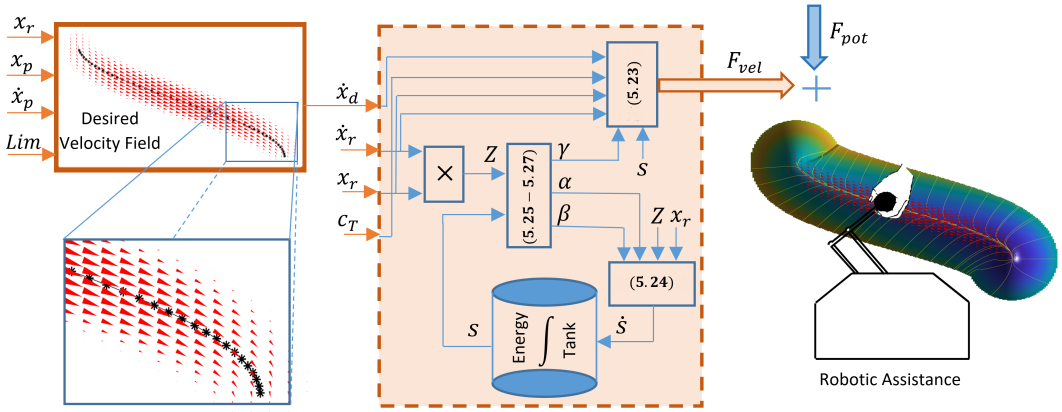

Figure 5.6: Illustrates the proposed velocity field controller in Section. 5.3. In each position (x_r), the desired velocity is calculated from the demonstrated velocity (x_p, $\dot{x}_p$), then forwarded to the variable dissipative field controller with the energy tank to be followed passively. Finally, the force produced by the velocity field controller (F_{vel}) is added to the force produced by the potential field function (F_{pot}) to provide assistance to the patient to accomplish the task without therapist intervention

tate based on the desired velocity direction ($\widehat{\nu_T} = \frac{\dot{x}_d(x_r)}{||\dot{x}_d(x_r)||}$) and span the desired velocity tangential-normal space as,

$$D(x_r) = Q(x_r)\ C\ Q(x_r)^T \tag{5.20}$$

$$Q(x_r) = [\widehat{\nu_T}\ \widehat{\nu_{N_1}}\ ...\widehat{\nu_{N_n}}] \tag{5.21}$$

$$C = \begin{bmatrix} c_T & & 0 \\ & c_{N_1} & \\ & & \ddots \\ 0 & & c_{N_{n-1}} \end{bmatrix} \tag{5.22}$$

In (5.20), $D(x_r)$ denotes the position-based varying damping matrix, $Q(x_r)$ represents the eigenvector matrix that transforms diognal eigenvalue matrix (C) to inertial Cartesian coordinates. In (5.21), $\widehat{\nu_T}$ represents the normalized tangential direction vector, and $\{\widehat{\nu_{N_1}}, ..., \widehat{\nu_{N_n}}\}$ are the normalized arbitrary and orthogonal vectors normal to the desired velocity. The eigenvalues c_T and $\{c_{N_1}, ..., c_{N_n}\}$ in (5.22) represent the tunable damping parameters in tangential

and normal directions to the desired velocity, respectively. Having the variable damping matrix, the velocity field controller in (5.6) is

$$F_{vel}(x_r, \dot{x}_r) = -D(x_r)(\dot{x_r} - \gamma(Z,S)\dot{x}_d(x_r)) = \\ - D(x_r)\dot{x_r} + \gamma(Z,S)c_T\dot{x}_d(x_r) \quad (5.23)$$

$\dot{x}_d(x_r)$ is an eigenvector of $D(x_r)$ with corresponding eigenvalue c_T. Therefore, $D(x_r)\dot{x}_d = c_T\dot{x}_d(x_r)$ in (5.23). $\gamma(Z,S) \in R^+$ is the stabilizing energy tank scalar function, which is discussed later below. The velocity field controller damps the motion normal to the desired velocity (tuned by $\{c_{N_1}, ..., c_{N_n}\}$) but regulates the velocity tangent to the desired velocity $\dot{x}_d(x_r)$. If the patient is following the trajectory more slowly than the desired velocity, the controller will actively push (assist) the patient to go faster. If the patient is going faster than the desired velocity, the controller would resist and dissipate the energy. The tangent velocity deviation tolerance can be tuned by the therapist through the tangential damping parameter c_T.

The velocity field controller with its variable position-based damping matrix $D(x_r)$ can induce active energy to the system which can threaten the stability of the system even in interaction with passive environments. As suggested in [46], energy tank is suggested to tackle the non-passivity of the system. Energy tank refers to an additional state that stores the dissipative energy of the system (instead of wasting it) and uses this stored energy to induce it back to the system when active control action is required. Therefore, the energy tank state $S \in R$ is

$$\dot{S} = \alpha(S)\dot{x}(x_r)D(x_r)\dot{x}(x_r) - \beta(Z,S)c_T Z \quad (5.24)$$

in which $Z = \dot{x}(x_r)^T \dot{x}(x_d)$ and

$$\alpha(S) = \begin{cases} 1 & \text{if } S < \overline{S} \\ 0 & \text{otherwise} \end{cases} \tag{5.25}$$

Also,

$$\beta(Z, S) = \begin{cases} 0 & \text{if } S \leq 0 \ \& \ Z \geq 0 \\ 0 & \text{if } S \geq \overline{S} \ \& \ Z \leq 0 \\ 1 & \text{otherwise} \end{cases} \tag{5.26}$$

where the $\dot{S}$ represents the rate in which the energy tank is charging (positive rate) or depleting (negative rate). the $\dot{x}(x_r)D(x_r)\dot{x}(x_r) \in R^+$ term is always positive as the damping matrix $D(x_r)$ is positive definite. This is the dissipated passive energy that charges the energy tank and is controlled by a scalar multiplier $\alpha(S)$. $\alpha(S)$ is set to zero if the tank reaches its maximum energy level ($\overline{S}$) as in (5.25). In (5.24), $Z = \dot{x}(x_r)^T \dot{x}(x_d)$ indicates that the velocity field controller tangential velocity tracker is either active ($Z > 0$) or passive ($Z < 0$). $\beta(Z, S)$ is the scalar controller that will be zero, if the energy tank is depleted ($S \leq 0$) and the tracker needs more energy from the energy tank for active control action ($Z \geq 0$). Or if the energy tank is full ($S \geq \overline{S}$) and the tracker is passive and charging the tank with more energy ($Z > 0$). Now, the scalar function $\gamma(Z, S)$ in (5.23) is set to produce controlling action when energy tank is depleted as

$$\gamma(Z, S) = \begin{cases} \beta(Z, S) & \text{if } Z \leq 0 \\ \geq \beta(Z, S) & \text{if } Z \geq 0 \end{cases} \tag{5.27}$$

now, having both the potential field and velocity field controller with its energy tank stabilizer, the stability of the proposed framework can be investigated.

Lets define the candidate Lyapunov function as

$$\nu(x_r, \dot{x}_r) = \frac{1}{2}\dot{x}_r^T M \dot{x}_r + U(x_r) + S \tag{5.28}$$

which consists of the kinetic, potential and tank energy in the system. The proposed energy function $\nu(x_r, \dot{x}_r)$ is a positive definite function based on (5.1), (5.9) and (5.24). The time derivative of $\nu(x_r, \dot{x}_r)$ is

$$\dot{\nu}(x_r, \dot{x}_r) = \dot{x}_r^T M \ddot{x}_r + \frac{1}{2}\dot{x}_r^T \dot{M} \dot{x}_r + \dot{x}_r^T \nabla U(x_r) + \dot{S} \tag{5.29}$$

$M\ddot{x}_r$ is found by rearrangement of robot dynamic (5.1), replacing the equivalent control force (F_C) from (5.6), (5.7) and (5.23). Also, substituting $\dot{S}$ from (5.24) yields

$$\begin{aligned}\dot{\nu}(x_r, \dot{x}_r) = \dot{x}_r^T [&F_{pa} + F_{ext} - \nabla U(x_r) - D(x_r)\dot{x}_r \\ &+ \gamma(Z,S) c_T \dot{x}_d(x_r) - C(x_r, \dot{x}_r)\dot{x}_r - G(x_r) - f(\dot{x}_r)] \\ &+ \frac{1}{2}\dot{x}_r^T \dot{M} \dot{x}_r + \dot{x}_r^T \nabla U(x_r) + \alpha(S)\dot{x}(x_r) D(x_r) \dot{x}(x_r) \\ &- \beta(Z,S) c_T \dot{x}(x_r)^T \dot{x}(x_d)\end{aligned} \tag{5.30}$$

Rearranging the terms and considering the skew symmetric property of $\dot{M} - 2C(x_r, \dot{x}_r)$, we have

$$\begin{aligned}\dot{\nu}(x_r, \dot{x}_r) &= \dot{x}_r^T [F_{pa} + F_{ext}] - [1 - \alpha(S)] \dot{x}_r^T D(x_r) \dot{x}_r \\ &\quad + [\gamma(Z,S) - \beta(Z,S)] c_T Z - \dot{x}_r^T f(\dot{x}_r) \\ &= \dot{x}_r^T [F_{pa} + F_{ext}] - \eta(x_r, \dot{x}_r, Z, S) \\ &\leq \dot{x}_r^T [F_{pa} + F_{ext}]\end{aligned} \tag{5.31}$$

5.4 Experimental Evaluation

The proposed framework is experimentally evaluated using a Quanser rehabilitation robot (Quanser Consulting Inc., Markham, Canada). A force sensor (Gamma SI-32-2.5, from ATI Inc, Goodworth, NC, USA) was connected to the end-effector in order to measure the interaction force applied by the therapist to the patient as shown in Fig. 5.7. The parameters in Table. 5.1 are used in the system. Three different scenarios have been considered to evaluate the performance of the proposed potential and velocity field controllers in point-to-point position and impedance-based motions. Most of the daily tasks can be decomposed into point-to-point motion or impedance-based primitives. The main symptoms of cerebral palsy which are stiffness in joints and muscles, weakness and tremor (Section. 2.1.1) were simulated by spring arrays and transcutaneous electrical nerve stimulation of an adult without disability (author) to assess the capability of the system.

$K_{min} = 200$ $lim = 0.03$	$K_{max} = 600$ $c_N = 20\ N.sec/m$	$\sigma = 0.02$ $c_T = 20\ N.sec/m$	$\overline{S} = 20$ height

Table 5.1: The selected system parameters

5.4.1 Simulation of CP symptoms using spring arrays

Spring arrays were used to roughly simulate the muscle stiffness and incoordination in patients with CP. This approach eased the evaluation of the proposed framework and comparison of results with different tuning parameters, considering the passivity and consistency of the spring array. For the first experiment, a 2-dimensional point-to-point motion was expected. As shown in Fig. 5.7 The spring model (which represents a patient with stiff muscles) was expected to simply move the robotic end-effector from the starting point (A) to the target point (B) directly. As seen in Fig. 5.7, the spring array equilibrium point was

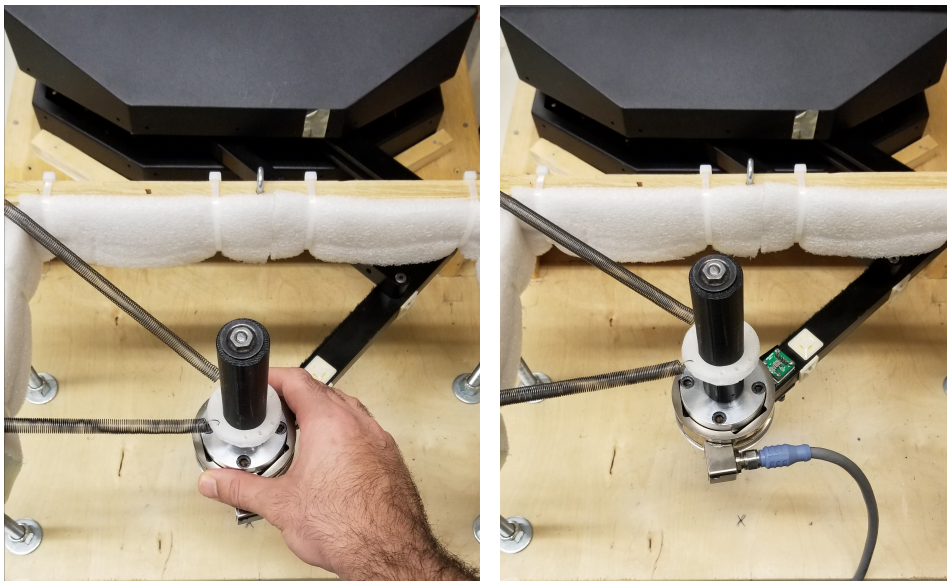

Figure 5.7: This figure depicts the experiment setup for experiment 1 in both demonstration (Left) and robotic assistance (right) phases. Spring array is used for simulation of spastic symptoms of CP in Section. 5.4.1

close to the point A, therefore it could not complete the task and move toward point B without assistance. Thus, a therapist (the author in this experiment) provided assistance and grabbed the robot end effector (connected to the spring array) and dragged it to the point B. Then, using the system parameters (Table. 5.1), the potential and velocity fields were learned as displayed in Fig. 5.8 to replicate the helpers demonstrated trajectory (i.e., position), velocity and interaction force. Now, using the potential field function gradient (5.7) and velocity field controller(5.23), the robotic assistance was provided to the spring array in five trials. In these trials, the robotic manipulator (connected to the robot end effector) was released in five different locations to highlight the convergence of the model in the task environment and evaluate the performance of the model and controllers to replicate the demonstrated velocity and interaction force.

As illustrated in Fig. 5.8, in all trials, the learned model successfully attracted the robotic manipulator towards point B. However, as the spring array was exerting force in $-X_1$ and X_2 directions, it can be observed that the

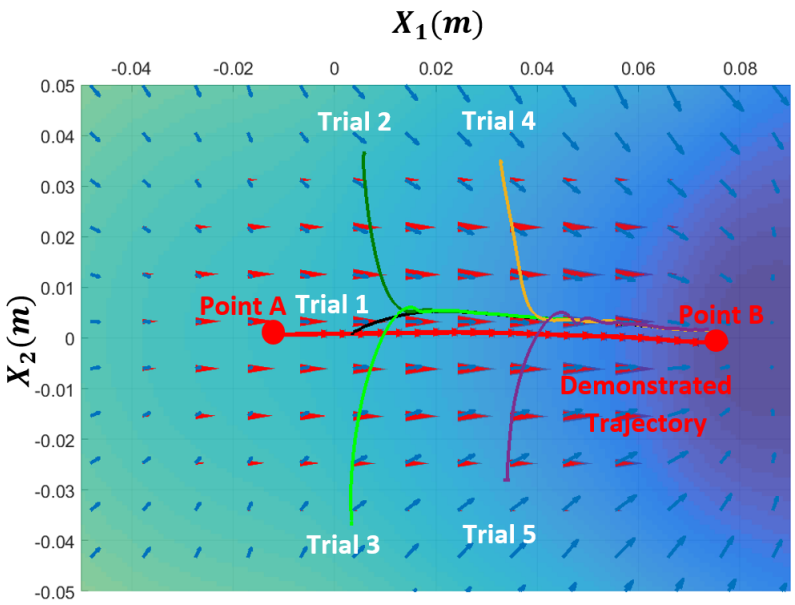

Figure 5.8: Illustrates the learned potential field function in Experiment 1 with blue colors giving the magnitude (the darker the color, the lower the potential value) and arrows indicating the direction of the force in each position. The red line is the demonstrated trajectory by the therapist from point A to point B. The red arrows demonstrate the velocity field along the trajectory. As seen in this figure, in all five trials, the potential field attracted the robotic manipulator to the trajectory and then to point B.

robotic manipulator deviation from the demonstrated trajectory in those directions. The level of deviation from the demonstrated trajectory can be adjusted by tuning K_{min} and K_{max} parameters. The higher the stiffness parameters, the lower the deviation from demonstrated trajectory (i.e. lower freedom and contribution for the patient in task execution).

Fig. 5.9(a) illustrates the velocity in X_1 direction in demonstration phase and five reproduction trials. As the proposed controller is time-independent, the tracking performance of controllers should be analyzed spatially. In this experiment, we provided high damping behavior in the environment (Table. 5.1) to further evaluate the performance of the velocity field controller to cope with force perturbation. This damping behavior in the task environment was not present in the demonstration phase, therefore the learned interaction force captured in the potential field falls short to accelerate the robot enough to

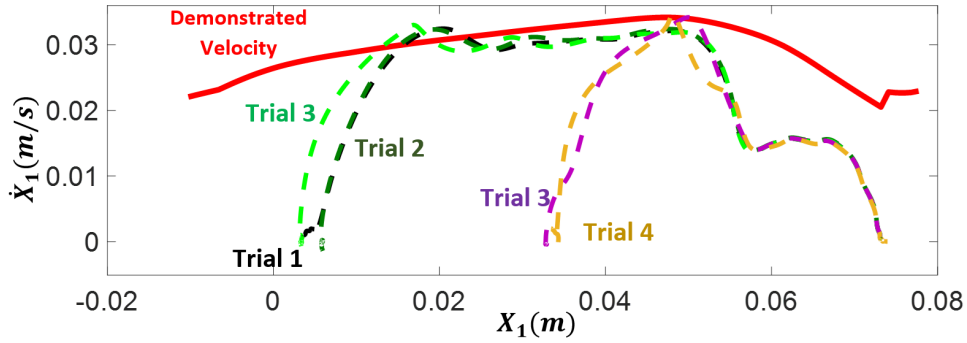

(a)Velocity

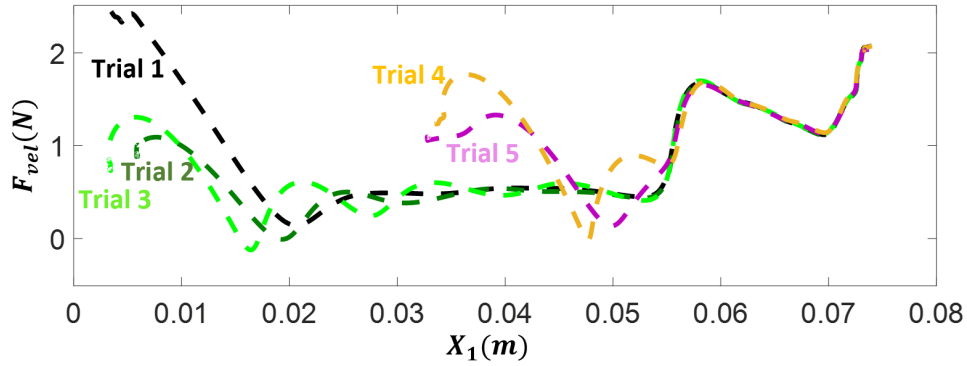

(b)Velocity field controller

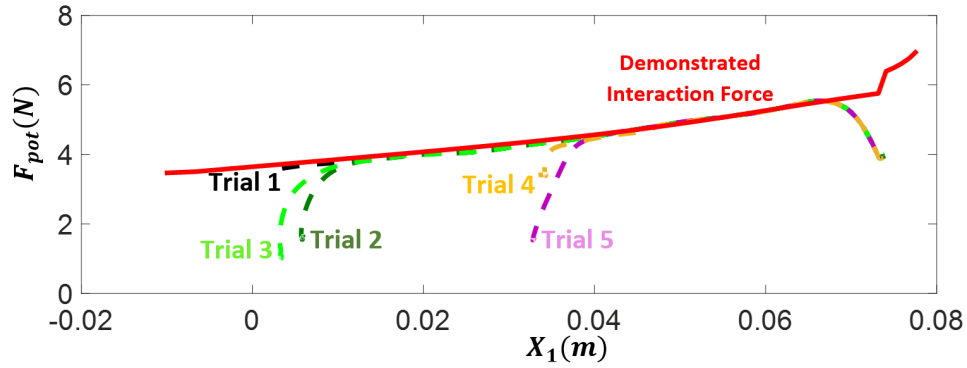

(c)Potential Field Function Force

Figure 5.9: (a) Depicts the velocity tracking for Experiment 1, with the vertical and horizontal axis representing the position and velocity in X_1 direction. As observed, the system assisted the spring array to reach the desired velocity in each position (as demonstrated by red color). (b) Depicts the force produced by the velocity field controller F_{vel}. (c) illustrates the interaction force by the potential field function F_{pot} in X_1 direction. As soon as the robotic manipulator is attracted to the trajectory the potential field function exerted identical interaction force as seen in the demonstration phase (red plot).

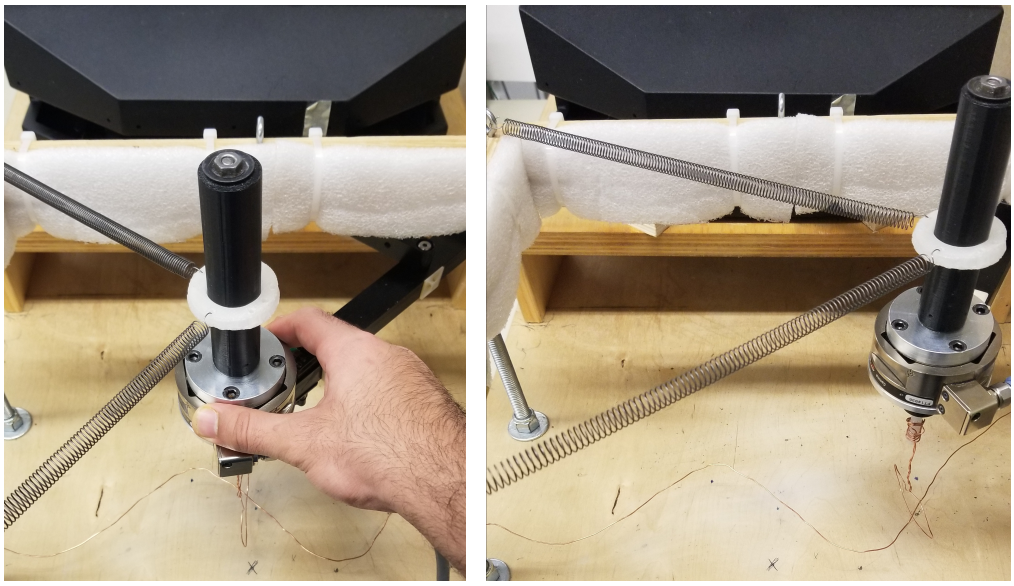

Figure 5.10: This figure depicts the experiment setup for experiment 2 in both demonstration (Left) and robotic assistance (right) phases.

reach the desired velocity demonstrated. As sketched in Fig.5.9(a), due to the dampness (i.e., dissipation) of the environment, static friction of the system and transient response of the controller, the robot manipulator slowly converged to the demonstrated velocity and compensated for the force perturbation in the environment. At the end of the trajectory, the desired velocity field is set to zero to prevent the shift in the convergence point of the potential field.

The potential field is learned to provide the same interaction force in the tangential direction as observed in the demonstration phase. Fig.5.9(c) shows the interaction force exerted by the potential field (F_{pot}) in X_1 direction which is perfectly identical to the demonstrated interaction force as soon as the robot is attracted to the vicinity of the trajectory.

The velocity field controller F_{vel}, as illustrated in Fig.5.9(b), mainly exerted positive assistive force in the same direction to the motion to compensate the dampness in the environment. At the beginning and end of the motion, the velocity field controller made up for the inertia and static friction in the system and accelerated the robotic manipulator to reach the desired velocity. Also, at

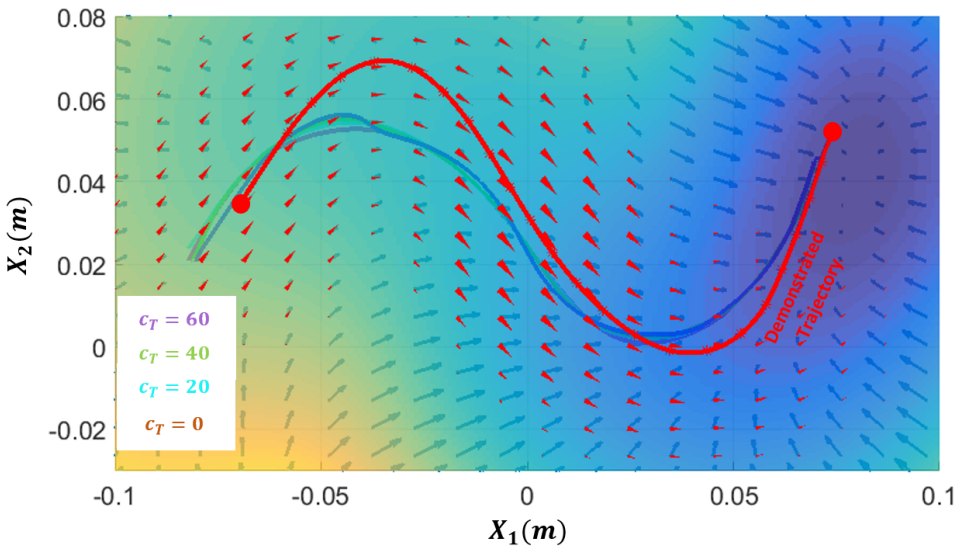

Figure 5.11: Depicts the velocity field and learned potential field around the demonstrated trajectory from point A to point B in experiment 2. The system successfully assisted the spring array to move the loop along the wire from point A to point B without hitting the wire in all 4 trials with different c_T parameter

the end of the motion, F_{vel} increased to compensate for the drop in the F_{pot}.

In experiment 2 with spring models, the aim was to evaluate the performance of the velocity field controller and how it can be tuned to adjust the level of patient's (simulated by a spring model in this experiment) deviation from demonstrated velocity. As demonstrated in Fig.5.10, the task was a simple "wire in the Loop game", a loop was connected to the robot's end effector, which was going along a wire in the task environment. The game was completed successfully if the patient can moved the loop from point A to point B, without any direct contact between the loop and the wire.

The robot equilibrium point was close to point A and it was unable to accomplish the task without assistance. In the next phase the helper assisted and grabbed the robot end effector with the attached loop along the wire all the way to the point B. Then the demonstrated assistance with its position, velocity and interaction force data was captured by potential and velocity field as Fig.5.11. Finally, in the robotic assistance phase, the task is performed

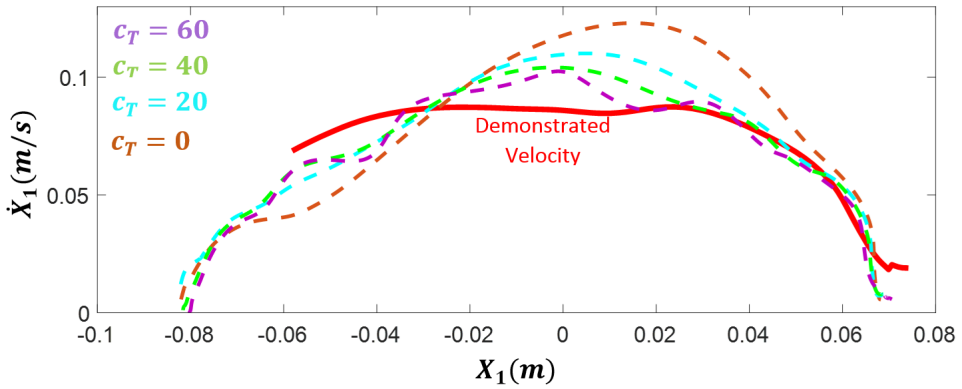

(a)Velocity

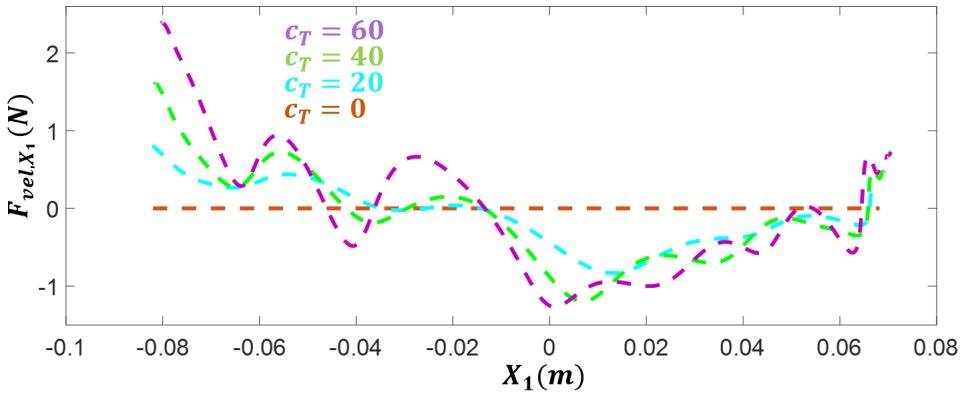

(b)Velocity field controller

Figure 5.12: (a) Depicts the observed velocity tracking in X_1 direction in all four trials with different c_T in experiment 2. As seen, the velocity tracking of demonstrated velocity (red plot) got more accurate as the c_T parameter increased . (b) The control signal produced by velocity field controller F_{vel} in X_1 direction increased as the c_T parameter increased

successfully by the robotic assistance (without helpers intervention) in four trials.

The dampness in the environment in the robotic assistance phase was small (same as the demonstration phase, Table. 5.1), also due to the deviation of the spring array from the demonstrated trajectory the interaction force to the robotic manipulator was more than the one demonstrated and we expected higher velocities at the end of the trajectory, Fig.5.12(a) and Fig.5.13(a) with $c_T = 0$. In order to evaluate the performance of velocity field controller in velocity regulation with its c_T parameter in each trial, a different value for

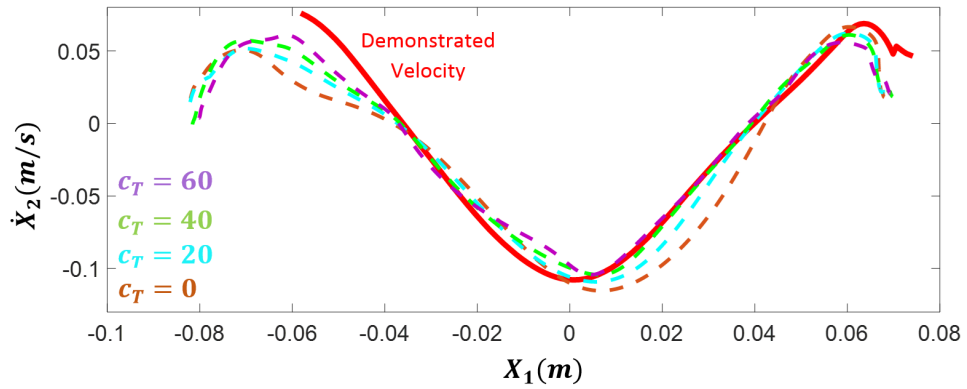

(a)Velocity

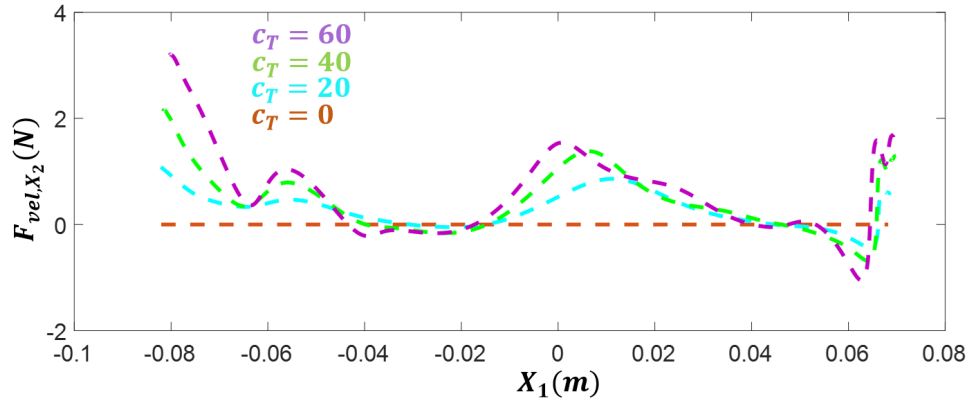

(b)Velocity field controller

Figure 5.13: (a) The observed velocity tracking in X_2 direction in all four trials with different c_T in experiment 2. The velocity tracking of demonstrated velocity (red plot) got more accurate as the c_T parameter increased. (b) The control signal produced by velocity field controller F_{vel} in X_2 direction increased as the c_T parameter increased

c_T was assigned. As illustrated in Fig.5.13 and Fig.5.12, the higher the c_T parameter, the higher the control force from the velocity field controller and the lower the deviation from the demonstrated velocity.

Fig.5.12(a) and Fig.5.13(a) illustrate that in the first phase of the motion, due to inertia and static friction of the system, the robotic manipulator (connected to the spring array) was going slower than the demonstrated velocity in both X_1 and X_2 directions. Therefore, the velocity field controller exerted an assistive force (in the direction of the motion) as seen in Fig.5.12(b) and Fig.5.13(b) to accelerate the robotic manipulator to reach the desired velocity.

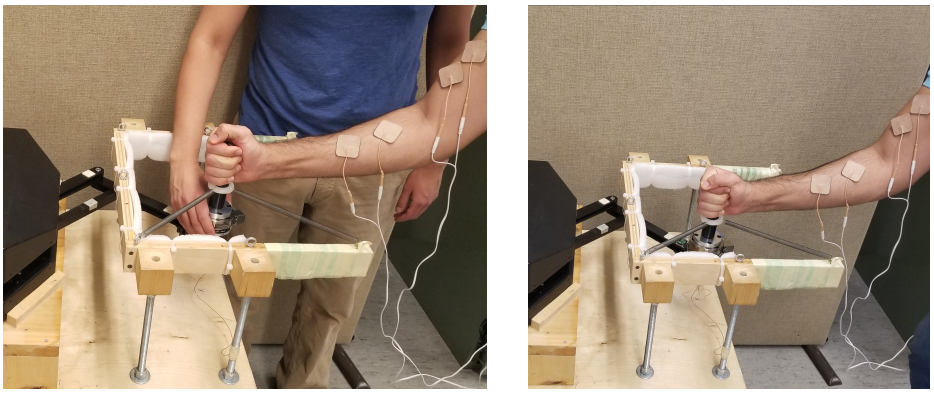

Figure 5.14: depicts the experiment setup for experiment 3 in both demonstration (Left) and robotic assistance (right) phases. Two pairs of transcutaneous electrical nerve stimulation pads were used for simulation of CP symptoms in Section. 5.4.2

In the second phase, the velocity becomes more than the demonstrated velocity in both directions, therefore, the velocity field controller provided resistive force (in opposite direction to the motion) to decrease the velocity.

5.4.2 Using Transcutaneous Electrical Nerve Stimulation (TENS)

To simulate incoordination and involuntary motions (that is a common symptom of people with CP) in a person without a disability (author), a transcutaneous electrical nerve stimulation (TENS) was utilized. Low-frequency stimulation of upper arm and wrist muscles induced a similar behavior observed in a patient with CP [18]. In this experiment, the task was the same "wire in the Loop" game with connected spring array to the end effector. Then the patient (author with TENS) was expected to move the loop with the spring array from point A to point B without hitting the wire. Due to the connected spring array, the task was "impedance-based" as the patient should exert a specific force in each position along the trajectory to reach the same velocity. The aim of this experiment was to evaluate the system in presence of normal interaction

forces and observe the energy tank performance to save up the passive dissipative energy and use it for active control action. Fig.5.14 demonstrates the experimental set-up in the demonstration and robotic assistance phases. In the demonstration phase, a research assistant (called therapist in the reminder of this section) provided assistant to the patient in a single task execution. The task was divided into two sections. In the first section of the trajectory the TENS unit was on, therefore the user exerted a sinusoidal force (tremor like) in X_2 direction. In the second section of the trajectory, the TENS unit was off so the user required minimal assistance from the helper to perform the rest of the task and reach point B.

Fig.5.15(a) and Fig.5.16(a) illustrate the acquired data from the therapist assistance in cooperative task demonstration. As observed, the patient required minimal assistance in the second section of the trajectory as the muscle stimulation is off. Thus, the interaction force in the normal and tangential directions were around zero. In normal direction, the stiffness matrix is linearly mapped to the demonstrated normal interaction force from the therapist to replicate the provided assistance in an as needed paradigm, Fig.5.16. Thus, the stiffness matrix would be around K_{min}. In tangential direction (Fig.5.15), the low interaction force results in low tangential gradient (i.e., Force) in the potential field around the trajectory (5.13).

The velocity field controller with its energy tank mechanism ensured the stability and passivity of the overall system. In section 1 of the trajectory, due to muscle stimulation, the patient exerted sinusoidal forces in the normal direction and deviated the trajectory. The velocity field controller damped the patient's energy in the normal direction and saved it up in the energy tank state S as shown in Fig.5.18.(a) and Fig. 5.18.(b)). Then, uses this energy in section 2 of the trajectory to actively regulate the deviation of the patient to the demonstrated velocity along the trajectory.

With stiffness mapping to normal interaction force, and modified convex

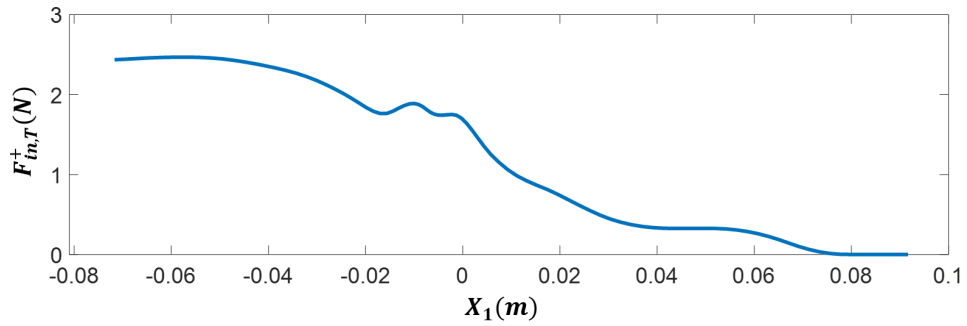

(a)Demonstrated tangential interaction force

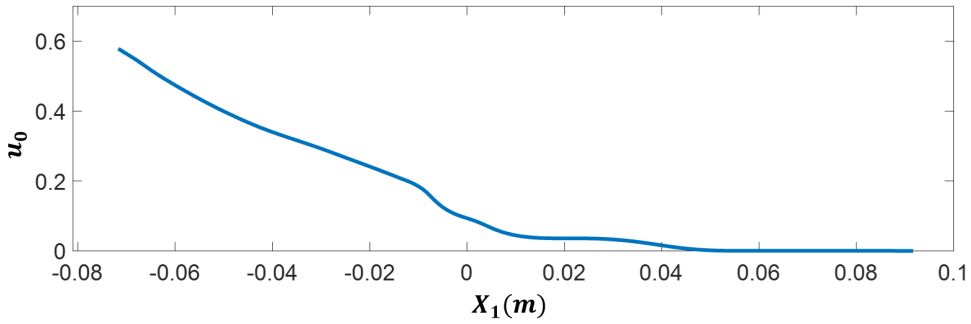

(b)Learned bias potential parameter

Figure 5.15: (a) Depicts the demonstrated tangential interaction force in X_1 direction. (b) The bias potential parameter u_0 is learned to replicate the demonstrated tangential interaction force, using a convex optimization algorithm (5.14)

optimization to adjust the tangent slope (i.e., gradient) of the potential field based on the demonstrated tangential interaction force. The potential field was learned Fig.5.17(a). As illustrated, the low stiffness and gradient in section 2 of the trajectory cause flat potential field around the trajectory. Still, the velocity field controller regulated the velocity and assist/resist the patient if they were going under/over the demonstrated velocity in both sections.

In the robotic assistance phase, using the parameters in Table. 5.1, The robotic system failed to provide the required performance and the deviation caused by the user in the normal direction in section 1 of the trajectory exceeded the loop radius (1.5 cm) (Fig.5.17). Tuning the stiffness parameter and multiplying the K_{min} and K_{max} by three ($3K_{min}$, $3K_{max}$), the potential field slope around the trajectory got steeper, thus patient's movements got more

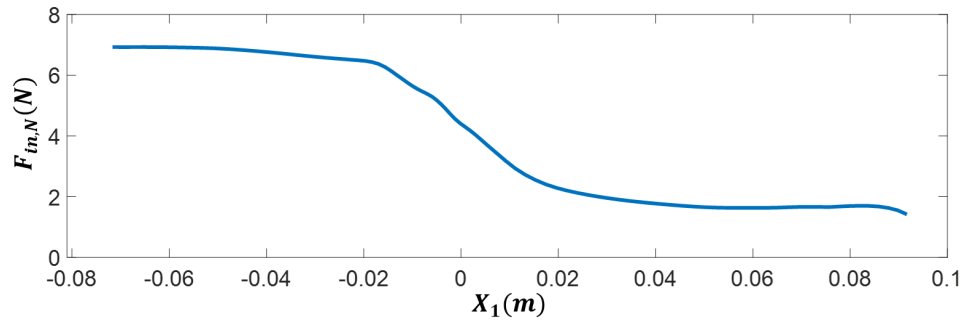

(a)Demonstrated normal interaction force

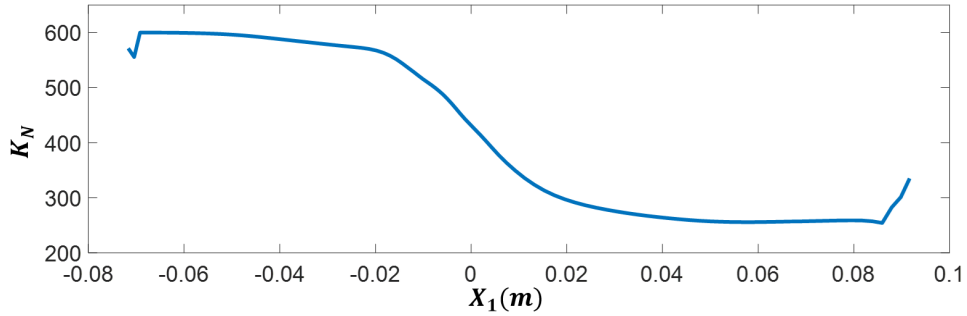

(b)Stiffness parameter

Figure 5.16: (a) Depicts the demonstrated normal interaction force in X_1 direction (b) The stiffness parameter K_N^i which was linearly mapped from the demonstrated normal interaction force so that the system restrict the user around the trajectory based on the force observed in demonstration phase.

restricted normal to the trajectory. With the new stiffness parameter, the patient was assisted to follow the trajectory more accurately and complete the task successfully.

All in all, the proposed framework with potential field function and velocity field controller captured simultaneously the trajectory, impedance, interaction force and velocity of the demonstrated trial by the therapist and effectively reproduced it passively.

5.5 Conclusion

The proposed learning from demonstration framework for robotic assistance can have applications in various tasks that involve cooperative human-robot task execution. However, without the loss of generality, an application for

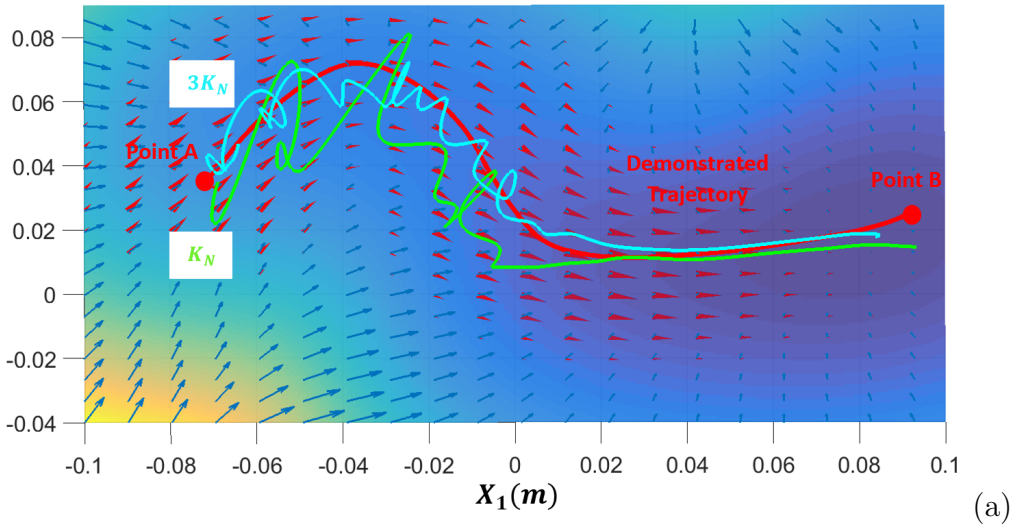

(a)

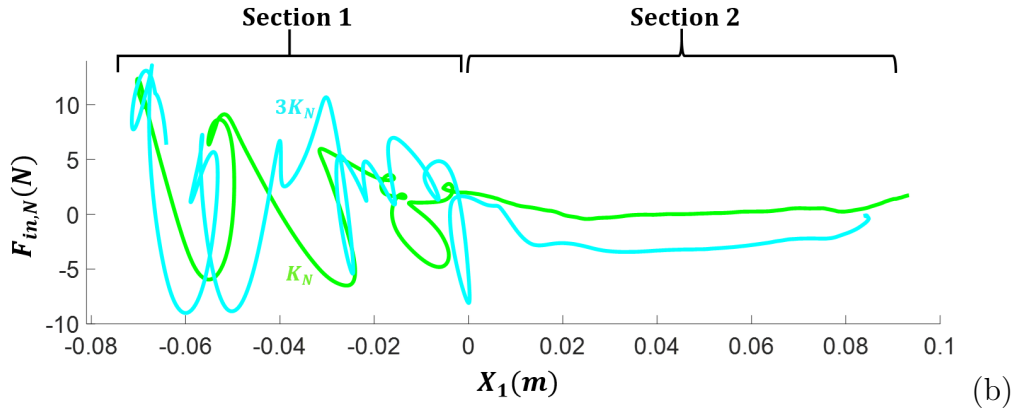

(b)

Figure 5.17: (a) Illustrates the potential and velocity field around the trajectory in experiment 3. As demonstrated with $\{K_{N,min} = 200 and K_{N,max} = 600$ (K_N) $\}$ the user deviation from the trajectory was high and he failed to complete the task (the loop hits the wire), by tuning the parameters to $\{K_{N,min} = 600 and K_{N,max} = 1800$ $(3K_N)$ $\}$ the system restricted the user around the trajectory for accurate task execution. (b) depicts the normal interaction force of the user.

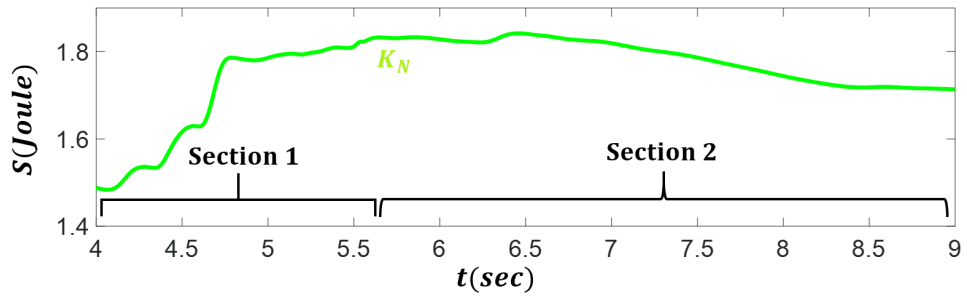

(a)Energy Tank with $K_{min} = 200$ and $K_{max} = 600$

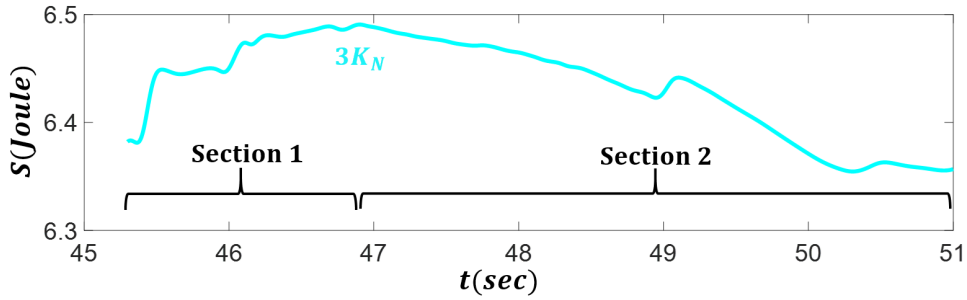

(b)Energy Tank with $K_{min} = 600$ and $K_{max} = 1800$

Figure 5.18: Shows the energy tank state (S) charging up in section 1 of the trajectory as the user's energy was damped in normal direction, and discharges in section 2 of the trajectory as the velocity field controller spent it for active control action.

assist-as-needed assistance to people with disability has been the main focus in this paper. The framework, with its potential field function and velocity field controller, was modified and developed to reproduce the helper's assistance (i.e., trajectory, impedance, velocity, interaction force) in the robotic assistance phase. The efficacy and performance of the system were evaluated in three scenarios involving spring arrays (to simulate muscle stiffness in CP) and a healthy adult induced with CP symptoms (tremor), using transcutaneous electrical nerve stimulation.

Chapter 6

Conclusion & future work

In this thesis, two class of learning from demonstration frameworks for assistive robotic systems have been proposed and implemented practically: 1) Time-indexed motion learning 2) Position-indexed motion learning. While these frameworks can have a plethora of applications in cooperative human-robot task execution, without the loss of generality, a potential application in assistive robotic systems for children with cerebral palsy (CP) and assist-as-needed rehabilitation was discussed.

Only a short intervention (demonstration) of a helper was enough to learn the required task-specific assistance and reproduce it without his/her intervention. Therefore the robotic manipulator saved the helper's time. These systems could also provide us with valuable sensory data to evaluate the user's performance and learn their unique execution and behavioral characteristic.

Time-indexed motion learning form demonstration was used in **Chapter 3** and **Chapter 4** to develop the assistive robotic system. In these frameworks, the Gaussian mixture model was utilized to capture the position-time data acquired from the therapist-patient cooperative demonstration. Then in the robotic assistance phase, Gaussian mixture regression extracted the expected position with its average and variability in each time-index. Also, a proposed tangential-normal impedance controller was used to regulate the

human-robot interaction tangent and normal to the demonstrated trajectory as the robotic manipulator follows the expected trajectory with time. The more the impedance parameters, the less the patient's freedom to deviate from the trajectory.

In **Chapter 3** the impedance parameters (in tangential and normal direction) were non-variable and tuned based on the maximum required assistance along the trajectory (i.e., minimum variability between the demonstrated trajectories). The system was experimentally evaluated performing a simple pick and place game through a teleoperation system (master-slave) in a 2-dimensional environment. A spring array was used to represent a child with CP and model the spastic symptom of CP. In the demonstration phase, the therapist holding the slave robot (that was in task environment) assisted the spring array that was in contact with the master robot to go from point A to point B. Then in the robotic assistance phase, the system provided the learned assistance to the spring array to perform the task in eight trials with different values for tangential and normal impedance parameters. Then a set of parameters were chosen to provide the minimum assistance required to reach the box B. However this level of assistance is constant along the trajectory, even though it is not required in all sections of the trajectory.

In **Chapter 4**, the controller in **Chapter 3** was extended by proposing the tangential-normal varying impedance controller (TNVIC). In this controller, the impedance parameters in tangential and normal directions were also changing in magnitude with an inverse correlation to the variability observed in demonstrated trajectories. In experimental evaluation, an adult with induced CP symptoms (using transcutaneous electrical nerve stimulation) was asked to move the robotic manipulator from point A to point B through two gaps with different width without hitting them. The task is projected on an LCD screen placed under the robotic manipulator. The demonstration was done with both therapist and user (adult with induced CP symptoms) performing

the point-to-point motion task. Then in the robotic assistance phase, the system provided the user with learned assistance in times where it was needed (i.e., AAN) by regulating the impedance parameters inversely proportional to the demonstrated variability. Less variability was assumed as the requirement for more accuracy.

The time-indexed motion learning frameworks in **Chapter 3** and **Chapter 4** are time-dependent as the name implies. Thus the system works open-loop in trajectory generation for the interacting user to follow. These systems are not only prone to temporal perturbation but also can induce a high amount of force to the user if the distance between the robotic manipulator and robortic end effector increases (due to the connecting impedance model). To face these problems in **Chapter 5** we proposed position-indexed motion learning using potential field function and velocity field controller.

In **Chapter 5**, the non-parametric potential field function and the convex optimization algorithm used for learning the model, were both modified to simultaneously capture the demonstrated: 1) trajectory; 2) Impedance properties of therapist-patient interaction and 3) Therapist's assistive force along the trajectory. A velocity field controller was also proposed to regulate the damping (in the normal direction) and velocity (in tangential direction). The velocity field controller with its virtual energy tank state ensures the passivity of the overall system in interaction with a passive environment. The energy tank stores the damped energy and uses it for active control action in the controller. This time-independent framework was experimentally evaluated in three different scenarios involving spring arrays and an adult with transcutaneous electrical nerve stimulation inducing symptoms of CP. The system efficiently captured the demonstrated assistance and provided it in the reproduction phase to complete the designed tasks successfully with efficient trajectory, assistive force and velocity tracking of demonstration data. The system was robust to both spatial and temporal perturbations and stable because of the energy tank mechanism.

In the future, the main focus of our work will be to:

1. Evaluate the performance of the proposed frameworks in studies with children with CP.

2. Add an adaptive law to the proposed TNVIC in **Chapter 4**) to adapt the interaction dynamics to the user's hand in tangential and normal directions.

3. Develop reinforcement learning algorithms to update the GMM (for time-indexed motion learning in **Chapter 3** and **Chapter 4**) and potential field function (for position-indexed motion learning in **Chapter 5**) based on the user's interactive performance in task execution. Therefore the trajectory and robotic assistance in both tangential and normal directions can adapt to user's performance which can be different from the demonstration phase (e.g., patient gets tired or enhances his/her performance by repetition).

4. Find an algorithm to generalize several of the therapist's demonstrated assistance in the task environment and learn the required potential and velocity fields in **Chapter 5**, for any point to point motion in that environment, without the need for any new therapist demonstration.

Bibliography

[1] JS. Shilt LA. Koman, BP. Smith BP. Cerebral palsy. *Lancet*, 33:1619–1631, 2004.

[2] R. W. Armstrong. Definition and classification of cerebral palsy. *Developmental Medicine and Child Neurology*, 49:1–44, 2007.

[3] Nigel Paneth, Ting Hong, and Steven Korzeniewski. The descriptive epidemiology of cerebral palsy. *Clinics in perinatology*, 33(2):251–267, 2006.

[4] J. Robert PT. Palisano M. Orlin K. Suzann, PT. Campbell. *Physical Therapy for Children*. 2002.

[5] J. Suoranta M. Mkel A. Malmivaara H. Anttila, I. Autti-Ramo. Effectiveness of physical therapy interventions for children with cerebral palsy: A systematic review. *BMC Pediatrics*, 8, 2008.

[6] E. J. Gibson. Exploratory behavior in the development of perceiving, acting, and the acquiring of knowledge. *Annual review of psychology*, 39: 1–41, 1988.

[7] Boris Gindis. The social/cultural implication of disability: Vygotsky's paradigm for special education. *Educational Psychologist*, 30(2):77–81, 1995. doi: 10.1207/s15326985ep3002_4. URL https://doi.org/10.1207/s15326985ep3002_4.

[8] Mohammad Najafi, Mojtaba Sharifi, Kim Adams, and Mahdi Tavakoli. Robotic assistance for children with cerebral palsy based on learning from tele-cooperative demonstration. *International Journal of Intelligent Robotics and Applications*, pages 1–12.

[9] Mohammad Najafi, Kim Adams, and Mahdi Tavakoli. Robotic learning from demonstration of therapist's time-varying assistance to a patient in trajectory-following tasks. In *International Conference on Rehabilitation Robotics (ICORR)*. IEEE, 2017.

[10] M. Maaref, A. Rezazadeh, K. Shamaei, and M. Tavakoli. A gaussian mixture framework for co-operative rehabilitation therapy in assistive impedance-based tasks. *IEEE Journal of Selected Topics in Signal Processing*, 10(5):904–913, Aug 2016. ISSN 1932-4553. doi: 10.1109/JSTSP.2016.2532847.

[11] M. Maaref, A. Rezazadeh, K. Shamaei, R. Ocampo, and T. Mahdi. A bicycle cranking model for assist-as-needed robotic rehabilitation therapy using learning from demonstration. *IEEE Robotics and Automation Letters*, 1 (2):653–660, July 2016. ISSN 2377-3766. doi: 10.1109/LRA.2016.2525827.

[12] Seyed Mohammad Khansari-Zadeh and Oussama Khatib. Learning potential functions from human demonstrations with encapsulated dynamic and compliant behaviors. *Autonomous Robots*, 41(1):45–69, 2017.

[13] Federica Ferraguti, Cristian Secchi, and Cesare Fantuzzi. A tank-based approach to impedance control with variable stiffness. In *IEEE International Conference on Robotics and Automation*, pages 4948–4953. IEEE, 2013.

[14] E. Blanche. Play in children with cerebral palsy: Doing withnot doing to. pages 375–393, 12 2008.

[15] J. Piaget. *The origins of intelligence in children*. International Universities Press, New York, 1952.

[16] B. Sutton-Smith. *The ambiguity of play*. Harvard University Press, London, 2001.

[17] Adriana Ríos-Rincón, Kim Adams, Joyce Magill-Evans, and Al Cook. Playfulness in children with limited motor abilities when using a robot. *Physical & Occupational Therapy in Pediatrics*, 36(3):232–246, 2016.

[18] Isao Sakamaki, Kim Adams, Maria Fernanda Gomez Medina, Javier Leonardo Castellanos Cruz, Nooshin Jafari, Mahdi Tavakoli, and Heidi Janz. Preliminary testing by adults of a haptics-assisted robot platform designed for children with physical impairments to access play. *Assistive Technology*, 0(0):1–9, 2017. doi: 10.1080/10400435.2017.1318974. URL https://doi.org/10.1080/10400435.2017.1318974. PMID: 28696831.

[19] Noelia Chia Bejarano, Serena Maggioni, Laura De Rijcke, Carlos Cifuentes G., and David J. Reinkensmeyer. *Robot-Assisted Rehabilitation Therapy: Recovery Mechanisms and Their Implications for Machine Design*, volume 10. 01 2016. ISBN 978-3-319-24899-8.

[20] Laura Marchal-Crespo and David J. Reinkensmeyer. Review of control strategies for robotic movement training after neurologic injury. *Journal of NeuroEngineering and Rehabilitation*, 6(1):20, Jun 2009. ISSN 1743-0003. doi: 10.1186/1743-0003-6-20.

[21] N. Hogan. Impedance control: An approach to manipulation. In *1984 American Control Conference*, pages 304–313, June 1984.

[22] Mojtaba Sharifi, Saeed Behzadipour, and Gholamreza Vossoughi. Nonlinear model reference adaptive impedance control for humanrobot interactions. *Control Engineering Practice*, 32(Supplement C):9 – 27,

2014. ISSN 0967-0661. doi: https://doi.org/10.1016/j.conengprac.2014.07.001. URL http://www.sciencedirect.com/science/article/pii/S0967066114001713.

[23] Y. Mao and S. K. Agrawal. Design of a cable-driven arm exoskeleton (carex) for neural rehabilitation. *IEEE Transactions on Robotics*, 28(4): 922–931, Aug 2012. ISSN 1552-3098. doi: 10.1109/TRO.2012.2189496.

[24] M. Sharifi, S. Behzadipour, and G. R. Vossoughi. Model reference adaptive impedance control of rehabilitation robots in operational space. In *2012 4th IEEE RAS EMBS International Conference on Biomedical Robotics and Biomechatronics (BioRob)*, pages 1698–1703, June 2012. doi: 10.1109/BioRob.2012.6290690.

[25] L. Dipietro M. Ferraro J. Krol K. Rannekleiv H. I. Krebs, J. J. Palazzolo. Rehabilitation robotics: Performance-based progressive robot-assisted therapy. *Autonomous Robots*, 15(1):7–20, 2003. doi: 10.1023/A:1024494031121.

[26] A. V. Dowling, O. Barzilay, Y. Lombrozo, and A. Wolf. An adaptive home-use robotic rehabilitation system for the upper body. *IEEE Journal of Translational Engineering in Health and Medicine*, 2:1–10, 2014. ISSN 2168-2372. doi: 10.1109/JTEHM.2014.2314097.

[27] B. Ding, Q. Ai, Q. Liu, and W. Meng. Path control of a rehabilitation robot using virtual tunnel and adaptive impedance controller. In *2014 Seventh International Symposium on Computational Intelligence and Design*, volume 1, pages 158–161, Dec 2014. doi: 10.1109/ISCID.2014.204.

[28] T. Lozano-Perez. Robot programming. *Proceedings of the IEEE*, 71(7): 821–841, July 1983. ISSN 0018-9219. doi: 10.1109/PROC.1983.12681.

[29] Adam Coates, Pieter Abbeel, and Andrew Y. Ng. Learning for control

from multiple demonstrations. In *Proceedings of the 25th International Conference on Machine Learning*, ICML '08, pages 144–151, New York, NY, USA, 2008. ACM. ISBN 978-1-60558-205-4. doi: 10.1145/1390156.1390175. URL http://doi.acm.org/10.1145/1390156.1390175.

[30] S. S. M. Salehian, M. Khoramshahi, and A. Billard. A dynamical system approach for softly catching a flying object: Theory and experiment. *IEEE Transactions on Robotics*, 32(2):462–471, April 2016. ISSN 1552-3098. doi: 10.1109/TRO.2016.2536749.

[31] S. M. Khansari-Zadeh, K. Kronander, and A. Billard. Learning to play minigolf: A dynamical system-based approach. 2012.

[32] Jung-Hoon Hwang, Ronald Arkin, and Dong-Soo Kwon. Mobile robots at your fingertip: Bezier curve on-line trajectory generation for supervisory control. 2:1444 – 1449 vol.2, 11 2003.

[33] R. L. Andersson. Aggressive trajectory generator for a robot ping-pong player. *IEEE Control Systems Magazine*, 9(2):15–21, Feb 1989. ISSN 0272-1708. doi: 10.1109/37.16766.

[34] Jacopo Aleotti and Stefano Caselli. Robust trajectory learning and approximation for robot programming by demonstration. *Robotics and Autonomous Systems*, 54:409–413, 2006.

[35] D. Kulic, D. Lee, C. Ott, and Y. Nakamura. Incremental learning of full body motion primitives for humanoid robots, Dec 2008. ISSN 2164-0572.

[36] Dana Kuli, Wataru Takano, and Yoshihiko Nakamura. Incremental learning, clustering and hierarchy formation of whole body motion patterns using adaptive hidden markov chains. *The International Journal of Robotics Research*, 27(7):761–784, 2008. doi: 10.1177/0278364908091153. URL https://doi.org/10.1177/0278364908091153.

[37] Wiqas Ghai and Navdeep Singh. Literature review on automatic speech recognition. 41:42–50, 03 2012.

[38] S. Calinon, F. Guenter, and A. Billard. On learning, representing, and generalizing a task in a humanoid robot. *IEEE Transactions on Systems, Man, and Cybernetics, Part B (Cybernetics)*, 37(2):286–298, April 2007. ISSN 1083-4419. doi: 10.1109/TSMCB.2006.886952.

[39] S. Calinon and A. Billard. What is the Teacher's Role in Robot Programming by Demonstration? - toward Benchmarks for Improved Learning. *Interaction Studies. Special Issue on Psychological Benchmarks in Human-Robot Interaction*, 8(3), 2007.

[40] Baris Akgun, Maya Cakmak, Jae Wook Yoo, and Andrea Lockerd Thomaz. Trajectories and keyframes for kinesthetic teaching: A human-robot interaction perspective. In *Proceedings of the Seventh Annual ACM/IEEE International Conference on Human-Robot Interaction*, HRI '12, pages 391–398, New York, NY, USA, 2012. ACM. ISBN 978-1-4503-1063-5. doi: 10.1145/2157689.2157815. URL http://doi.acm.org/10.1145/2157689.2157815.

[41] Brenna Argall and Aude Billard. Learning from demonstration and correction via multiple modalities for a humanoid robot.

[42] T. K. Moon. The expectation-maximization algorithm. *IEEE Signal Processing Magazine*, 13(6):47–60, Nov 1996. ISSN 1053-5888. doi: 10.1109/79.543975.

[43] S. Calinon. *Robot Programming by Demonstration: A Probabilistic Approach*. Engineering sciences: Microtechnology. CRC, 2009. ISBN 9782940222315. URL https://books.google.ca/books?id=7l65QwAACAAJ.

[44] A. J. Ijspeert, J. Nakanishi, and S. Schaal. Movement imitation with nonlinear dynamical systems in humanoid robots. In *Proceedings 2002 IEEE International Conference on Robotics and Automation (Cat. No.02CH37292)*, volume 2, pages 1398–1403, 2002. doi: 10.1109/ROBOT.2002.1014739.

[45] S. M. Khansari-Zadeh and A. Billard. Learning stable nonlinear dynamical systems with gaussian mixture models. *IEEE Transactions on Robotics*, 27 (5):943–957, Oct 2011. ISSN 1552-3098. doi: 10.1109/TRO.2011.2159412.

[46] k Kronander and A Billard. Passive interaction control with dynamical systems. *IEEE Robotics and Automation Letters*, 1(1):106–113, 2016.

[47] Oussama Khatib. Real-time obstacle avoidance for manipulators and mobile robots. *The International Journal of Robotics Research*, 5(1):90–98, 1986. doi: 10.1177/027836498600500106. URL https://doi.org/10.1177/027836498600500106.

[48] E. Rimon and D. E. Koditschek. Exact robot navigation using artificial potential functions. *IEEE Transactions on Robotics and Automation*, 8 (5):501–518, Oct 1992. ISSN 1042-296X. doi: 10.1109/70.163777.

[49] James Kuffner and Jing" Xiao. *Motion for Manipulation Tasks*. Springer International Publishing, 2016. ISBN 978-3-319-32552-1.

[50] G. Ganesh, N. Jarrass, S. Haddadin, A. Albu-Schaeffer, and E. Burdet. A versatile biomimetic controller for contact tooling and haptic exploration, May 2012. ISSN 1050-4729.

[51] Djordje Mitrovic, Stefan Klanke, and Sethu Vijayakumar. Learning impedance control of antagonistic systems based on stochastic optimization principles. *The International Journal of Robotics Research*, 30(5): 556–573, 2011. doi: 10.1177/0278364910387653.

[52] B. Kim, J. Park, S. Park, and S. Kang. Impedance learning for robotic contact tasks using natural actor-critic algorithm. *IEEE Transactions on Systems, Man, and Cybernetics, Part B (Cybernetics)*, 40(2):433–443, April 2010. ISSN 1083-4419. doi: 10.1109/TSMCB.2009.2026289.

[53] Shuzhi Sam Ge, Yanan Li, and Chen Wang. Impedance adaptation for optimal robotenvironment interaction. *International Journal of Control*, 87(2):249–263, 2014. doi: 10.1080/00207179.2013.827799. URL https://doi.org/10.1080/00207179.2013.827799.

[54] David Braun, Matthew Howard, and Sethu Vijayakumar. Optimal variable stiffness control: formulation and application to explosive movement tasks. *Autonomous Robots*, 33(3):237–253, Oct 2012. ISSN 1573-7527. doi: 10.1007/s10514-012-9302-3. URL https://doi.org/10.1007/s10514-012-9302-3.

[55] Sylvain Calinon, Irene Sardellitti, and Darwin Caldwell. Learning-based control strategy for safe human-robot interaction exploiting task and robot redundancies. In *IEEE/RSJ International Conference on Intelligent Robots and Systems*, pages 249–254. IEEE, 2010.

[56] E. Gribovskaya, A. Kheddar, and A. Billard. Motion learning and adaptive impedance for robot control during physical interaction with humans. In *2011 IEEE International Conference on Robotics and Automation*, pages 4326–4332, May 2011. doi: 10.1109/ICRA.2011.5980070.

[57] K. Kronander and A. Billard. Stability considerations for variable impedance control. *IEEE Transactions on Robotics*, 32(5):1298–1305, Oct 2016. ISSN 1552-3098. doi: 10.1109/TRO.2016.2593492.

[58] John J. Craig. *Introduction to Robotics: Mechanics and Control*. Addison-Wesley Longman Publishing Co., Inc., Boston, MA, USA, 2nd edition, 1989. ISBN 0201095289.

[59] J. M. Dolan, M. B. Friedman, and M. L. Nagurka. Dynamic and loaded impedance components in the maintenance of human arm posture. *IEEE Transactions on Systems, Man, and Cybernetics*, 23(3):698–709, May 1993. ISSN 0018-9472. doi: 10.1109/21.256543.

[60] Sonia Chernova; Andrea L. Thomaz. *Robot Learning from Human Teachers*. 2014.

[61] Matteo Saveriano and Dongheui Lee. Learning motion and impedance behaviors from human demonstrations. In *1t1h International Conference on Ubiquitous Robots and Ambient Intelligence*, pages 368–373. IEEE, 2014.

[62] Gideon Schwarz. Estimating the dimension of a model. 6(2):461–464, 2017.

[63] Prevalence and characteristics of children with cerebral palsy in europe. *Developmental Medicine Child Neurology*, 44(9):633–640, 2002. ISSN 1469-8749. doi: 10.1111/j.1469-8749.2002.tb00848.x. URL http://dx.doi.org/10.1111/j.1469-8749.2002.tb00848.x.